

REPORT DOCUMENTATION PAGE			Form Approved OMB No. 0704-0188		
<p>Public reporting burden for this collection of information is estimated to average 1 hour per response, including the time for reviewing instructions, searching existing data sources, gathering and maintaining the data needed, and completing and reviewing this collection of information. Send comments regarding this burden estimate or any other aspect of this collection of information, including suggestions for reducing this burden to Department of Defense, Washington Headquarters Services, Directorate for Information Operations and Reports (0704-0188), 1215 Jefferson Davis Highway, Suite 1204, Arlington, VA 22202-4302. Respondents should be aware that notwithstanding any other provision of law, no person shall be subject to any penalty for failing to comply with a collection of information if it does not display a currently valid OMB control number. <b>PLEASE DO NOT RETURN YOUR FORM TO THE ABOVE ADDRESS.</b></p>					
1. REPORT DATE (DD-MM-YYYY) March 2013		2. REPORT TYPE Technical Paper		3. DATES COVERED (From - To) March 2013-May 2013	
4. TITLE AND SUBTITLE NEUTRAL ENTRAINMENT DEMONSTRATION IN A XENON FRC THRUSTER EXPERIMENT			5a. CONTRACT NUMBER FA9300-12-M-1503		
			5b. GRANT NUMBER		
			5c. PROGRAM ELEMENT NUMBER		
6. AUTHOR(S) Kirtley, D., Votroubek, G., Pancotti, A., Pihl, J., Slough, J.			5d. PROJECT NUMBER		
			5e. TASK NUMBER		
			5f. WORK UNIT NUMBER Q0W6		
7. PERFORMING ORGANIZATION NAME(S) AND ADDRESS(ES) Air Force Research Laboratory (AFMC) AFRL/RQRS 1 Ara Drive. Edwards AFB CA 93524-7013			8. PERFORMING ORGANIZATION REPORT NO.		
9. SPONSORING / MONITORING AGENCY NAME(S) AND ADDRESS(ES) Air Force Research Laboratory (AFMC) AFRL/RQR 5 Pollux Drive Edwards AFB CA 93524-7048			10. SPONSOR/MONITOR'S ACRONYM(S)		
			11. SPONSOR/MONITOR'S REPORT NUMBER(S) AFRL-RQ-ED-TP-2013-050		
12. DISTRIBUTION / AVAILABILITY STATEMENT Distribution A: Approved for Public Release; Distribution Unlimited. PA#13192					
13. SUPPLEMENTARY NOTES Conference paper for the JANNAF Space Propulsion Subcommittee meeting, Colorado Springs, CO, 29 April - 3 May 2013.					
14. ABSTRACT <p>The primary concern with operating a fully-ionized, plasma-based electric propulsion system on lightweight gasses is that the per-ion plasma formation and ejection losses are typically much larger than the energy of directed lightweight propellant. A new innovation, the PROTEAN, adds a secondary Neutral Entrainment (NE) stage that, if successful, can reduce the plasma formation losses. This NE stage injects neutral propellant into the plasma path after ejection from an electromagnetic Field Reversed Configuration (FRC) thruster, such as the 1 kW Electromagnetic Plasmoid Thruster (EMPT). The FRC ingests these neutral particles, accelerating them up to high velocities through resonant charge exchange collisions. The NE stage then highly efficiently adds further kinetic energy to the engorged plasmoid through Peristaltic Dynamic Acceleration, in which sequenced theta-pinch coils are actuated to provide a large magnetic pressure gradient. In total, this system should allow for the addition of active propellant mass without significant further ionization or plasma frozen flow losses. This paper presents the experimental and MHD modeling results of the Phase I PROTEAN program to demonstrate Neutral Entrainment in a 5 Joule conical experiment. Radial and temporal plasma profiles were measured using external and internal magnetic field probes and downstream time-of-flight langmuir probes for the formation, acceleration, and entrainment of a xenon FRC.</p>					
15. SUBJECT TERMS					
16. SECURITY CLASSIFICATION OF:			17. LIMITATION OF ABSTRACT	18. NUMBER OF PAGES	19a. NAME OF RESPONSIBLE PERSON Daniel Brown
a. REPORT Unclassified	b. ABSTRACT Unclassified	c. THIS PAGE Unclassified			19b. TELEPHONE NO (include area code) 661-525-5028

# NEUTRAL ENTRAINMENT DEMONSTRATION IN A XENON FRC THRUSTER EXPERIMENT

David Kirtley, George Votroubek, Anthony Pancotti, Jim Pihl  
MSNW LLC, Redmond, WA.

John Slough  
The University of Washington, Seattle, WA

## ABSTRACT

The primary concern with operating a fully-ionized, plasma-based electric propulsion system on lightweight gasses is that the per-ion plasma formation and ejection losses are typically much larger than the energy of directed lightweight propellant. A new innovation, the PROTEAN, adds a secondary Neutral Entrainment (NE) stage that, if successful, can reduce the plasma formation losses. This NE stage injects neutral propellant into the plasma path after ejection from an electromagnetic Field Reversed Configuration (FRC) thruster, such as the 1 kW Electromagnetic Plasmod Thruster (EMPT). The FRC ingests these neutral particles, accelerating them up to high velocities through resonant charge exchange collisions. The NE stage then highly efficiently adds further kinetic energy to the engorged plasmoid through Peristaltic Dynamic Acceleration, in which sequenced theta-pinch coils are actuated to provide a large magnetic pressure gradient. In total, this system should allow for the addition of active propellant mass without significant further ionization or plasma frozen flow losses. This paper presents the experimental and MHD modeling results of the Phase I PROTEAN program to demonstrate Neutral Entrainment in a 5 Joule conical experiment. Radial and temporal plasma profiles were measured using external and internal magnetic field probes and downstream time-of-flight langmuir probes for the formation, acceleration, and entrainment of a xenon FRC.

## INTRODUCTION

Electric Propulsion (EP) systems accelerate charged particles by the application of electrostatic and electrodynamic (magnetic) forces. In order to accelerate a propellant it must be charged and in typical electric propulsion systems it must undergo an ionizing collision event. The primary loss mechanism for all fundamental non-thermal electric propulsion devices and technologies is plasma formation loss [1]. In a realistic EP system, it takes 100-500 eV/per atom to take one neutral propellant particle and eject one ionized particle not counting kinetic energy addition. All plasma-based electrostatic or electromagnetic propulsion systems require an ionized particle to be able to accelerate propellant. Fundamentally, the energy cost of an ionizing collision is quite small, on the order of 10-20 eV. This would roughly correspond with an accelerating voltage of 10-20V for 50% efficiency. However, this is not a realistic assessment of the total energy required for ionization. In real plasma, energy losses also include recombination, excitation (radiation), and polarization. These effects will tend to dominate the effect of the ionizing collision, specifically at low energies. Figure 1 shows a compilation of energy loss mechanisms for an ideal plasma in argon and oxygen which have minimum energies of ~14 and ~16 eV/ion. It's clear that for electron temperatures below 50 eV, the minimum total ionization potential is much greater than 14-16 V. Neutral Entrainment attempts to minimize the largest energy loss of electromagnetic thrusters by effectively accelerating neutral propellant, without net ionization.

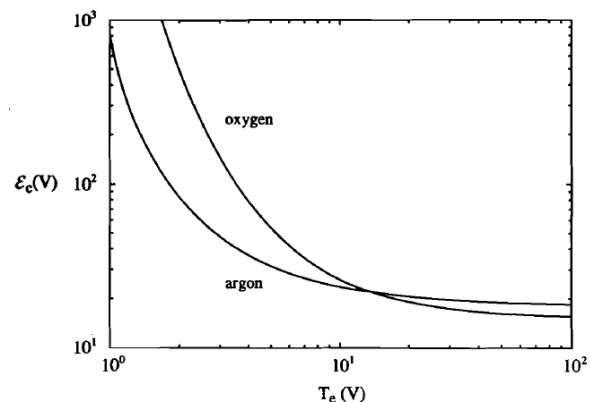


**Figure 1. Ionization energy cost, including excitation, as a function of electron temperature [2].**

## BACKGROUND OF PLASMA SOURCE

It is believed that a neutral entrainment system can operate with a variety of plasma sources, so long as that plasma is collisional and electromagnetically accelerated. For this experiment, a unique plasma source, a Field Reverse Configuration (FRC), was used which has closed field magnetic topology and relatively high plasma density. A FRC plasma consists of a closed field line, fully magnetized plasma with a large azimuthal current (as in Figure 2). The plasma diamagnetic current is generated opposite to the applied external field, creating a high-pressure configuration [3]. Typical FRC plasmas are formed with fast (few  $\mu\text{s}$ ), large ( $10$ 's of kA) inductive discharges.

The generation of FRCs using rotating magnetic fields (RMF) is well established [4]. The transverse rotating magnetic field is produced by external antennas as indicated in Figure 3. The first pair of loop antennas, carrying a sinusoidally oscillating current, produce a uniform magnetic field transverse to the coil axis as shown in black. A second loop pair produces a transverse magnetic field perpendicular to the first pair (blue) and are driven  $90^\circ$  out of phase with respect to the first pair. The composite magnetic field then forms a rotating, transverse magnetic field of constant magnitude. An electron magnetized to the field lines will rotate azimuthally on average at the same frequency as the antennas. An axial bias field is applied and, if the magnitude of the RMF induced  $J_\theta$  is sufficient to reverse this field, a true field reversed plasma is formed as in Figure 4. For an axially-distributed RMF system it is found that the azimuthal current is quite simply:

$$J_\theta = en_e \omega r$$

The PROTEAN source forms a RMF in a conical, gradient magnetic bias field. The large  $J_\theta$  is driven in a conical field with a radial magnetic field. The fully-formed FRC is then accelerated axially by the resultant  $J_\theta \times B_r$  force. The azimuthal current continues to be generated as the FRC moves downstream and the FRC accelerates throughout the entire cone. Finally, as the FRC expands through the conical section and beyond the exit of the cone, the thermal energy of the FRC is converted into axial velocity as in a typical magnetic expansion, resulting in a low temperature, high velocity, and compact plume. The key parameter that will be discussed is that the FRC current generates a self-magnetic field which supports a high internal plasma pressure. This pressure is in equilibrium with the external field and allows for magnetic compression and acceleration, as will now be described.

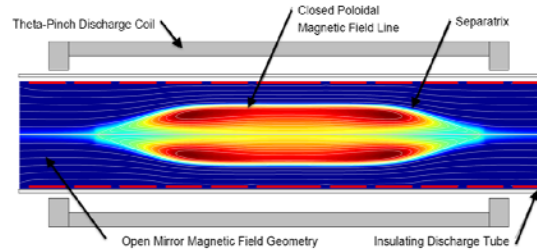


**Figure 2. Cross section of a cylindrical field reversed configuration plasma.**

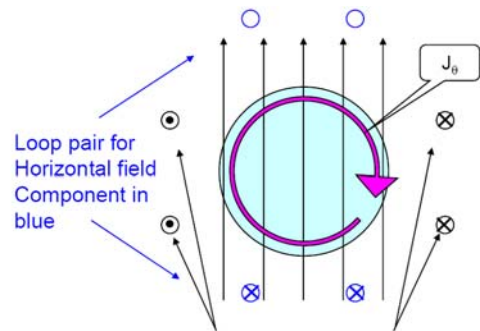


**Figure 3. Schematic of an RMF.**

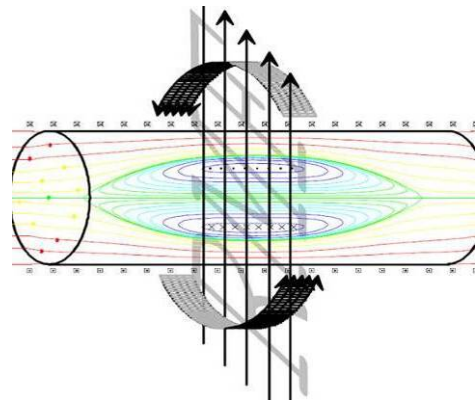
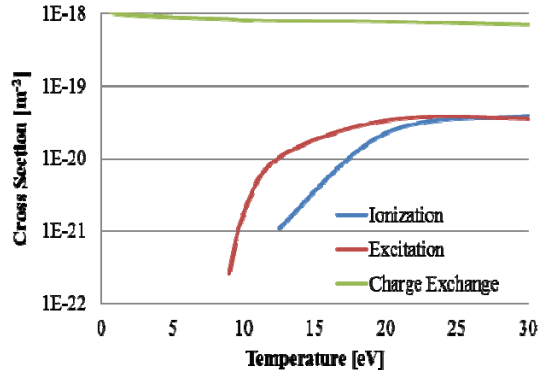


**Figure 4. Schematic of a Rotating Magnetic Field creating an FRC.**

## THE PHYSICS OF NEUTRAL ENTRAINMENT

The fundamental concept in Neutral Entrainment (NE) is that a FRC will ingest large quantities of neutral gas through charge exchange



collisions, not ionization. If one accelerates an FRC while providing upstream neutral gas, velocity can be specified and propellant mass added with very high efficiency. In recent FRC experiments it was found that accelerating an FRC into and through a large neutral population was beneficial to the FRC [5, 6]. It both gained mass and became more stable.

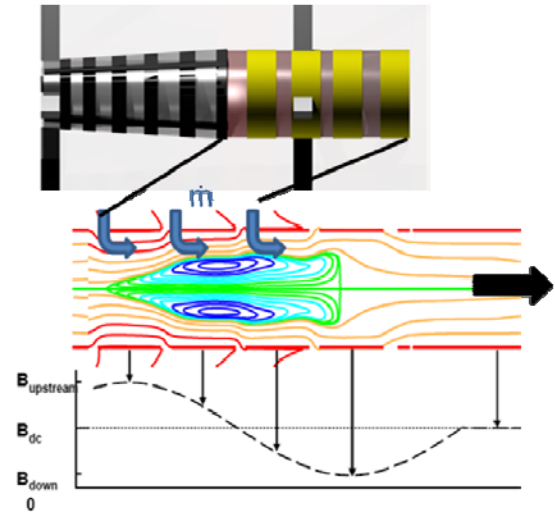


Figure 5. Neutral Entrainment ELF Thruster.

Neutral entrainment is believed to occur as follows. A collisional, ionized propellant is accelerated in a gradient magnetic field. In this specific case it will be in the form of a closed field, isolated FRC that is translating in a constant bias magnetic field. A slow, cold neutral gas population is introduced in front of the translating plasma. As the plasma ions collide with the neutral particles a positive ion will interact with an atom so as to capture a valence electron, resulting in a transfer of the electron from the atom to the ion. If this occurs between populations with the same mass, then the charge transfer occurs with *no* change in radial or axial momentum and no decrease in kinetic energy.

After this collision the resulting fast moving neutral particle proceeds out of the thruster unhindered by magnetic fields with its original momentum. Meanwhile, the slow-moving charged particle is *still confined in an accelerating magnetic field* and is subsequently accelerated to high velocity and applying a thrust force to the spacecraft (via magnetic field coils). In total, there are two fast moving, propellant particles but only one ionization loss, effectively reducing the total ionization loss per particle in half. Depending on the collision frequency, velocity, and density of the plasma and neutral populations this process will be repeated throughout an FRC and possibly several times. It is expected that there is a maximum of 10 neutral entrainments per particle possible with a typical NE geometry (simply due to the collision frequency for a typical geometry) reducing an ionization cost of 40 eV/ion to as low as 5 eV/ion, well below even the theoretical minima. Shown in Figure 5 is an MHD simulation of an accelerated FRC. The key parameter in this analysis is the ratio of ionization to charge exchange collision cross section. As is well known, the charge exchange collisions are much more likely than the ionization collisions [2].

Shown in Figure 6 are measured charge exchange and ionization cross sections for xenon. For the energies of interest charge exchange is 30+ times as likely as ionization. Finally, even if there is a 10% population of ionized propellant particles, they are accelerated with the propellant and are not considered to be a loss. Key design parameters are the mean free path for collisions for both charge exchange and neutral-neutral collisions for the length of the neutral entrainment region which determine the maximum number of entrainments. Additionally, a unique benefit of the plasma is that they typically do not relax to Maxwellian energy distributions and so the ionization potential of the high-energy electron tails is not realized [8].

Approved for public release; distribution is unlimited.

**Figure 6. Measured xenon Election Impact Ionization, Electron Ionization Excitation, and Charge Exchange cross section [6, 7].**

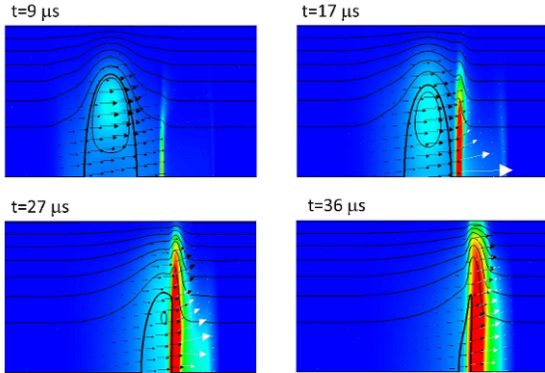


**Figure 7. Pressure pseudocolor plots for baseline ELF simulation. Neutral entrainment is shown by white arrows, contour is normalized neutral pressure.**

pressure. Finally, as one would expect, there is an increase in diamagnetism and a slowing of the FRC as it passes through the gas.

Figure 8 shows the temporal profile of the total momentum components of the FRC as well as the neutral population. Again, this is for a case in which the neutral mass was equal to the plasma mass. Quite obvious from these results is that both charge exchange and ionization play a critical role in these processes and that momentum can successfully be transferred to the neutral gas as desired. For an equal plasma to neutral mass, approximately 50% of the momentum of the plasma is transferred to the plasma, with a majority of that momentum transfer coming from charge exchange. In these cases, it appears that there is significant ionization of the background plasma although that energy appears to come from the initial thermal energy of the plasma rather than the kinetic energy, exactly as desired. While this not a loss mechanism in neutral entrainment, as the new plasma will be accelerated with the initial FRC plasma, it is less neutrals entrained overall, lessening the efficiency and T/P gain. It was found that this ionization ratio is a direct consequence of the plasma temperature at the exit of the thruster. For 5 eV total temperatures (similar to experiments) and high downstream neutral density, it was found that as low as 20% of neutrals are ionized while 80% of the plasma momentum is transferred to the neutrals.

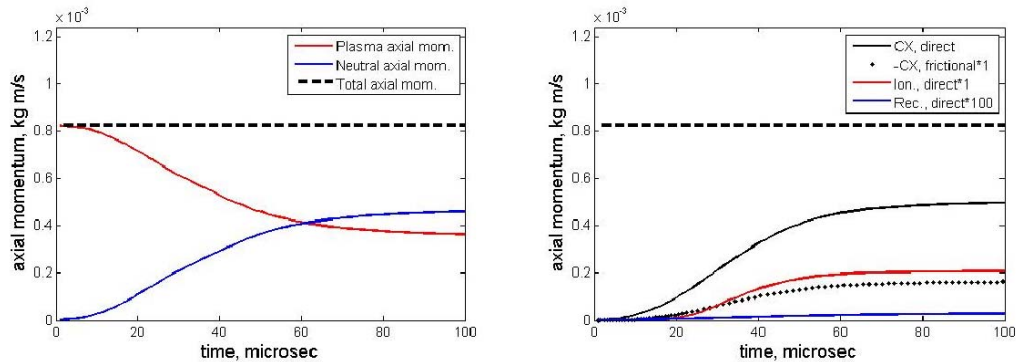


**Figure 8. Temporal profiles of momentum-related quantities for ELF baseline simulation**

Approved for public release; distribution is unlimited.

## BACKGROUND- PERISTALTIC DYNAMIC ACCELERATION (PDA)

Peristaltic dynamic acceleration is a concept that has been demonstrated in several FRC programs at MSNW LLC [11]. An FRC which is confined within a cylindrical magnetic field coil can be compressed or accelerated by that axial magnetic field. The key relation to dynamic magnetic acceleration is Equation 1, which relates the internal plasmoid density and temperature to the external magnetic pressure. This is for a magnetized, fully ionized plasma in radial equilibrium with the external field. The magnetic Beta shows the amount of compression of the FRC relative to the vacuum condition, where  $x_s$  is the normalized magnetic separatrix radius.

$$P_0 = n_0 kT = \frac{B_{ext}^2}{2\mu_0} \quad (1)$$

$$\langle \beta \rangle = \int_0^{x_s} \frac{2\mu_0 P}{B^2} dr = 1 - \frac{1}{2} x_s^2 \quad (2)$$

$$B_{ext} = \frac{B_{vac}}{(1 - x_s^2)} \quad (3)$$

Finally, for a plasma in radial equilibrium a relationship for magnetic flux conservation (Equation 2) equates the magnet flux during a compression cycle to flux after the plasmoid has been ejected. This can be directly translated into velocity and is demonstrated in the laboratory at very high efficiencies.

$$\frac{B_{ext}^2}{2\mu_0} (A_c - A_p) L_p - \frac{B_{vac}^2}{2\mu_0} A_p L_p = \frac{1}{2} M_p v_z^2 \quad (4)$$

The acceleration sequence can then be represented by Figure 5 which shows the magnetic flux contours for a translating FRC in a gradient field. In this simulation the FRC is formed earlier and then translated in the acceleration section. Three pulsed magnet field coils are triggered in sequence (typical accuracies <100 ns required) as the FRC translates. This creates a net magnetic field gradient behind the plasmoid accelerating it to high speeds. Additionally, a background field can be applied to act as a guide field, magnetic wall insulation, and to prevent reverse voltages from being applied to the charging capacitors. At this point the IGBT switches can be opened, recovering any stored inductive energy back to the capacitors. They are then recharged for the next discharge. The Inductive Plasmoid Accelerator used sequenced magnetic field coils to accelerate a theta-pinch formed FRC to greater than 300 km/s and required timing precision of less than 100 ns.

The MHD code MOQUI was used to model the dynamic acceleration of a set of post ejection acceleration coils. In MOQUI, an FRC was formed of similar densities and temperatures to the RMF-formed FRCs in EMPT. It was then allowed to travel into a conical section with a single active magnetic field coil. In Figure 9, the FRC was allowed to translate freely within the flux conserving region and appears to be a translating, well-formed FRC. In Figure 10, the downstream acceleration coil was activated, compressing and accelerating the plasmoid. From the figures it is clearly evident that the acceleration process occurs as expected, with the plasmoid increasing in velocity and the primary mass compressing radially as it accelerates axially.

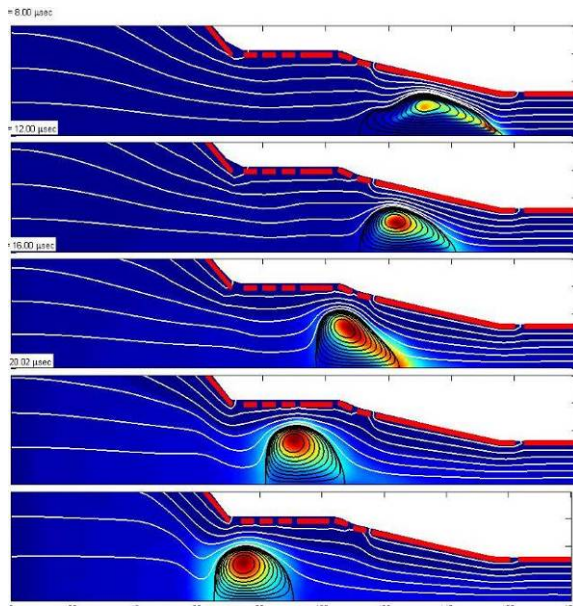


**Figure 9. An FRC translating without dynamic acceleration.**

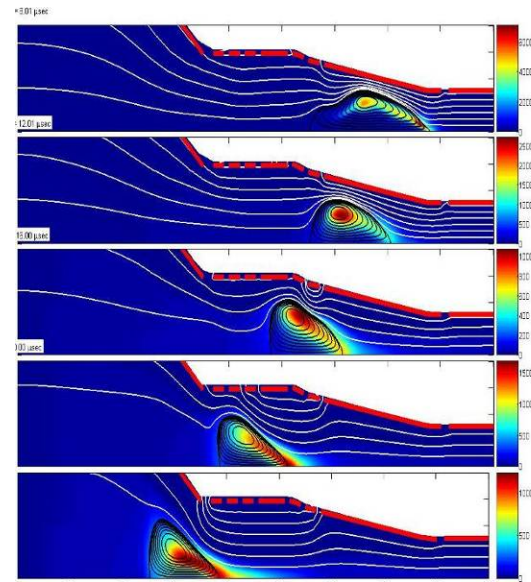


**Figure 10. An FRC translating with dynamic acceleration.**

## EXPERIMENTAL DESIGN

The experiment design is optimized for a 30 kW architecture and utilizes a conical quartz insulator, 28 cm long and 14 cm in outer, large diameter. The experiment has a total of ten accelerator coils axially along the entire length of the experiment setup as shown in Figure 12. These magnetic field coils integrate both the bias and accelerator fields for the RMF as well as the accelerator section. In this way the optimal balance of FRC formation, acceleration, and entrainment can be determined empirically without a preconceived reliance on the early model as timing can easily be prescribed. The insulator is a 12° quartz cone. There are five sets of external magnetic field and magnetic flux diagnostics along the length of the experiment. In this design there are no external flux conservers as there have been in previous thruster manifestations. In the PROTEAN the flux conserving boundary is established with the aforementioned multi-turn field coils. These twenty turn coils have an inductance ranging from 3 microhenry to 30 microhenry. The RMF antennas are scaled to 5 kW and placed externally to the accelerator coils. One of the critical innovations to this concept is the idea that FRC formation and ejection no longer has to be a passive process. The FRC plasma source plasma can be injected into the entrainment and acceleration section at the optimal density and plasma temperature, not necessarily the maximum acceleration pressure. In this way the optimal plasma conditions for neutral entrainment can be prescribed.

## GAS INJECTOR

One of the most complicated aspect of the PROTEAN experimental setup is the steady injection of neutral propellant to be entrained. In previous Neutral Entrainment research it was clearly shown that the geometric and temporal distribution of neutrals is critical to successful entrainment [12]. The neutrals must be located near the axis to prevent interaction with the quartz walls which leads to compression, and thus ionization of the neutrals. Additionally, the neutrals must be placed downstream of the FRC formation section, as the RMF is highly efficient at ionizing neutral gas, resulting in complete 40 eV/ion ionization of the propellant. Therefore, the special neutral injector was designed as shown in Figure 11 and Figure 13. In this design there are two propellant injection manifolds that can provide steady gas injection independently. The inner manifold is a Supersonic Molecular Beam Injector (SMBI) that uses a 400:1 expansion nozzle to accelerate and cool a neutral gas to extremely high velocities. This neutral gas flows steadily through the device and provides the downstream gas for entrainment. The secondary manifold uses a swirl-injected gas that has a high azimuthal gas velocity (relative to axial velocity) to lengthen its axial propagation. This swirled gas is used as the RMF-FRC formation propellant. In this design the slow moving gas fills the small end of the cone, while the fast moving gas fills the entire cone. The RMF ionizes and forms an FRC in the small, dense conical end. It then ejects (or is pushed with secondary acceleration coils) into the conical acceleration section, entraining neutrals and, ideally, lowering total effective frozen flow losses.



**Figure 11. Photograph of the high speed SMBI.**

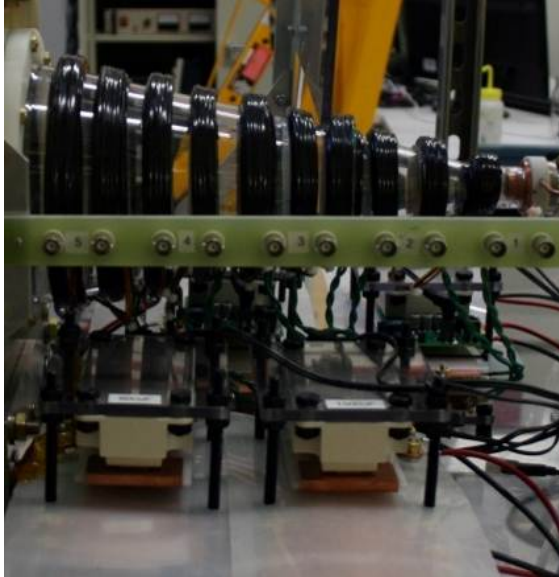


**Figure 12. Photograph of the PROTEAN test assembly.**

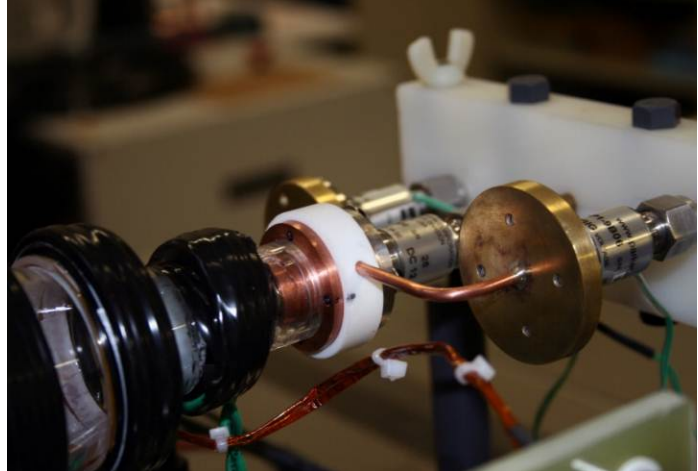


**Figure 13. Photograph of the high speed SMBI.**

An innovative combined circuit has been designed by the University of Washington such that the same accelerator coil can be used for both a bias field, as well as pulse high field acceleration. This circuit is the optimal design for combining an external, slow bias magnet field and a high speed pulsed accelerator field, all in the same magnetic coil and with minimum charging and circuit electronics. This circuit design will be detailed in later publications, however, the magnetic field and flux profiles given here utilize it. Throughout this research testing was initiated with vacuum magnetic field testing. The circuit was operated first with only bias field switches and was found to be well within design tolerances. Figure 14 and Figure 15 show the time history of magnetic field and magnetic flux for coil #1. Figure 16 shows magnetic flux profiles for four bias field configurations. The accelerator field coils were then added to the circuit with magnetic flux measurements for all the first accelerator coil group shown in Figure 17. Bias field rise times is set so that the RMF-formed plasma sees a constant magnetic field. The accelerator rise time is chosen such that magnetic field rise times corresponds to the translation time of the magnetized plasma.

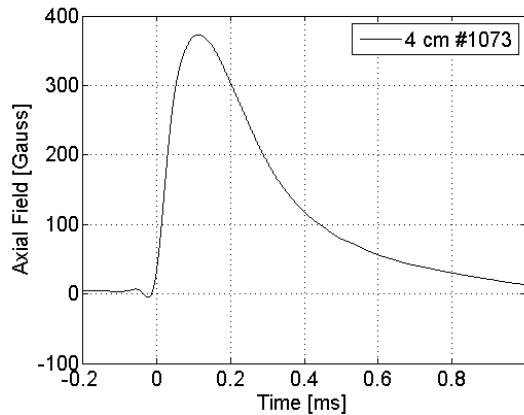


**Figure 14. Magnetic field history for the bias field discharge in coil 1.** Probe is located 4 cm from the base of the discharge insulator. Shot #1073.

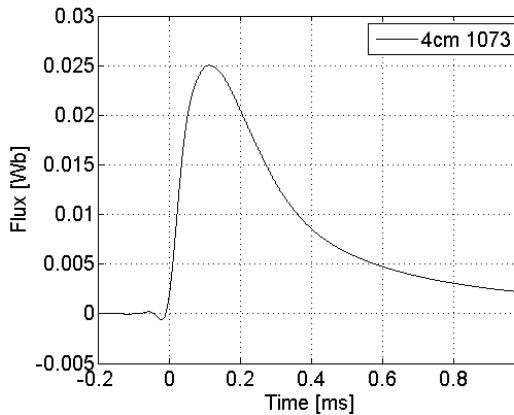


**Figure 15. Magnetic flux history for the bias field discharge in coil 1.** Probe is located 4 cm from the base of the discharge insulator. Shot #1073.

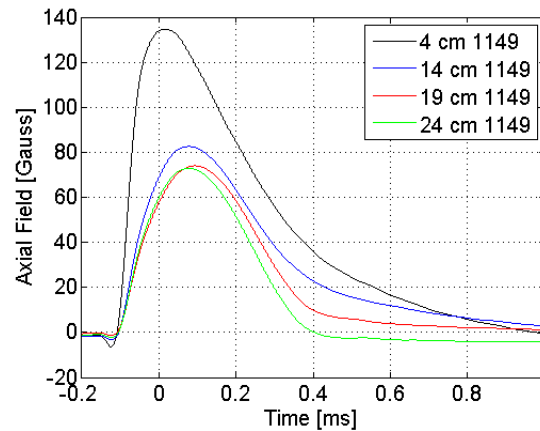


**Figure 16. Composite magnetic field profiles for all four bias field discharges.** Axial probe location is indicated. Shot #1149.

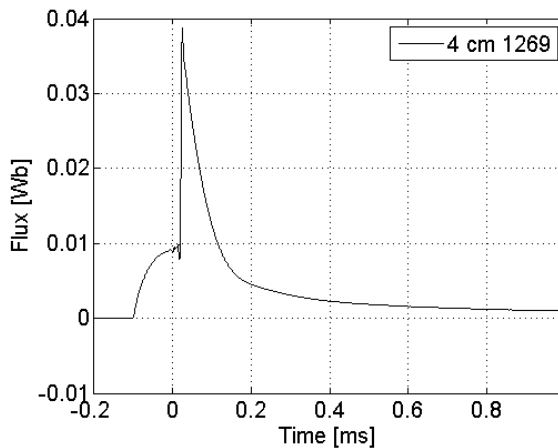


**Figure 17. Magnetic flux measurement with the primary accelerator coil.** Shown is 5 V bias and 100 V acceleration capacitor banks.

## XENON TESTING

A study of FRC formation using a xenon propellant and various propellant injection options were investigated. Using only the annular gas injection as was described earlier, a robust xenon FRC could be formed using RMF (Rotating Magnetic Field) formation at 1200 Volts. This is a total of 2.9 Joules and forms a well-coupled FRC. At the same gas pressure and puff valve settings, neutral gas was injected along the central axis.

In addition to the obvious entrainment effects expected, the addition of neutral gas also changes the dynamic behavior of FRC formation. The residual gas on axis from the free-streaming neutral injection is incorporated into the RMF FRC and acts as an additional source propellant for formation. As a result, for the same injection pressure and puff timing, the resulting FRC appears to be significantly enhanced with an increased ionization rate and resulting plasma pressure. Interestingly, this effect was not expected based off of larger FRC devices tested at MSNW which optimized with an annular gas injection.

In order to match the plasma conditions and FRC source conditions as closely as possible, the injection pressure for both the outer annular gas injection (to be called RMF propellant) and axial accelerated neutral propellant (to be called neutral entrainment propellant) was decreased. The results are shown in Figure 18, showing for all conditions well-formed RMF FRCs with rapid ionization and eventual ejection of the magnetized plasma are formed. When gas pressure was reduced in both propellant injectors to 15 psi, a similar gas condition for the plasma was reached, as compared with no injected gas. While identical diamagnetic signals were not found, this condition matched appropriately the plasma formation rate of ionization, growth within the discharge chamber region, and was similar in magnitude.

With a similarly matched formation condition, the downstream effects could now be analyzed. Shown in Figure 19 is the approximate plasma density as determined from an asymmetric double probe in ion saturation in supersonic flowing plasma. As is typical, the absolute error of these probes is quite large, though it is believed the relative error between operating conditions is within a few percent for variability for velocity and peak density were within 10% for these measurements. For clarity, error bars will not be shown, as they are not critical to this discussion.

Downstream results are quite clear and shown in Figure 19. When there is no neutral injection and RMF FRC is formed and accelerates through a constant flux expansion into the outer drift chamber. The ion velocity and density scale as expected with energy and the RMF propellant injected. With neutral entrainment injection, a similar FRC is formed and injected from the formation section. It then, however, quickly decelerates to a much slower speed arriving at the probe well over 100 microseconds later.

Radial profiles of plasma density for the first downstream probe are shown in Figure 20. Figure 20 shows a highly expanded FRC that was formed in a 4 cm radius cone expanded through a 7 cm radius cone and is drifting in a 14 cm cylindrical section. Plasma densities are as expected for this magnitude of expansion. Interestingly, the expected radial profile for plasma is seen with a lower density inner core and an approximate plasma radius of 8 cm. While this lower internal density is expected from RMF-formed FRCs, it is rarely seen downstream due to the relaxation, inward radial ion flow, and overall geometry expansion through a conical magnetic geometry. This annular geometry is most likely due to the significant annular gas injection and may suggest the reasoning for the increased performance with a more uniform gas distribution. Additionally, the FRC appears to be a coherent magnetized plasma object moving with a primary bulk velocity (shown by arrival time) as expected. A long exposure (250 ms) photograph of a xenon RMF FRC is shown in Figure 21.

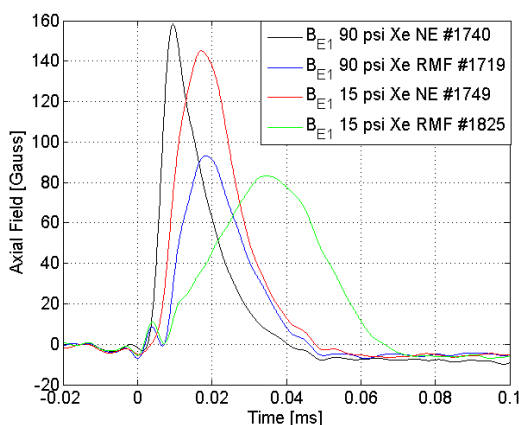


**Figure 18. RMF Formation with and without Neutral Entrainment propellant injection. Shot #'s as shown.**

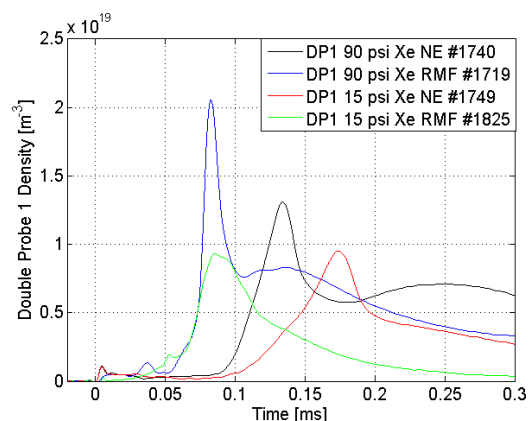


**Figure 19. Downstream double probe results for the key RMF formation conditions.**

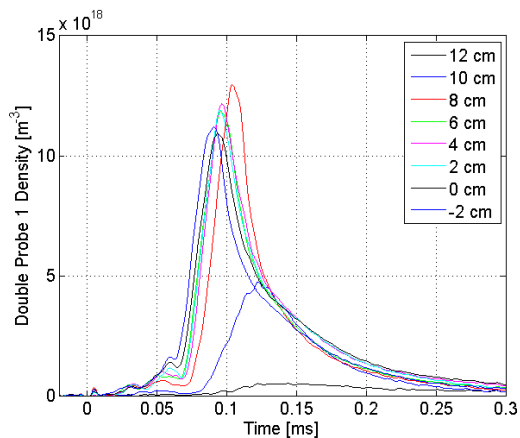


**Figure 20. RMF Radial profile. Shot #1770-1842.**

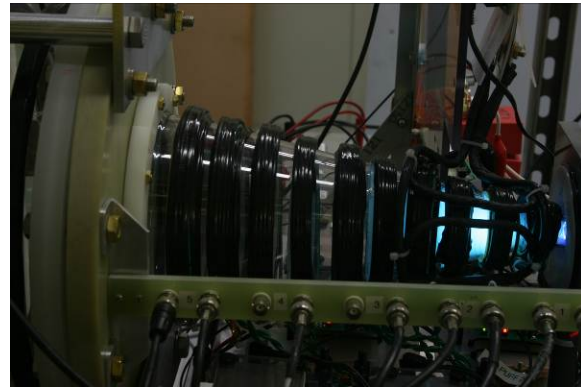


**Figure 21. Photograph of an RMF-xenon discharge at approximately 2.8 Joules. Annular pre-ionization and localized ionization region is clear.**

### NEUTRAL ENTRAINMENT WITH XENON

With the addition of the downstream on-axis neutral gas, shown in Figure 19, several key differences can be noted. Firstly, clear deceleration of the entire plasma body is seen. In addition, axial compression as well as increased radial deceleration and radial expansion are all obvious. These are expected effects as seen in the previous, referenced modeling efforts. This is markedly different from the fully ionized plasma body. A radial profile of the resulting plasma configuration is shown in Figure 22. The test geometry is shown again in Figure 23.

Additionally, the peak densities of the decelerated bodies are similar to the initial FRC and well within the probe error for supersonic plasma. Effects can be shown quite clearly that the xenon FRC appears to ionize less than what was seen in the neutral neon FRC studies performed earlier. Initial indications are that this is due to the lower electron temperature in the small-scale thrusters compared to the larger device tested previously [12]. Another difference with the neon results are that a central plasma density peak approximately 2 cm wide is evident, which is lower density, but high velocity. Rather than toroidal or ellipsoidal, the overall profile is wedge-shaped. This was not observed in either the modeling or previous neon results. Additionally, the peak appears to have drifted off axis from the plasma conditions. All of these results suggest the critical dependence on injected neutral gas and that this device would optimize towards an even higher density on axis that previously predicted or required for the lighter gases. Obvious entrainment and deceleration of the entire bulk plasma is seen.

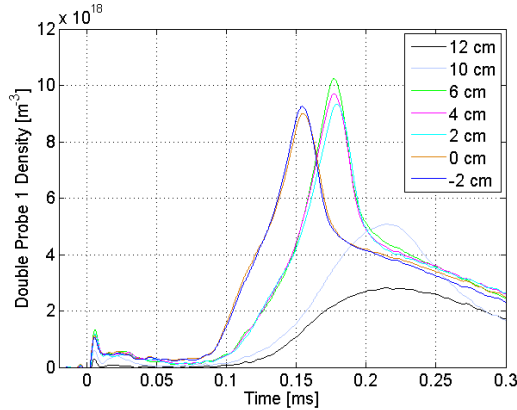


**Figure 22. Radial plasma profile for an RMF-formed xenon FRC interacting and decelerating in a passive, neutral background gas. Shot #1770-1842.**

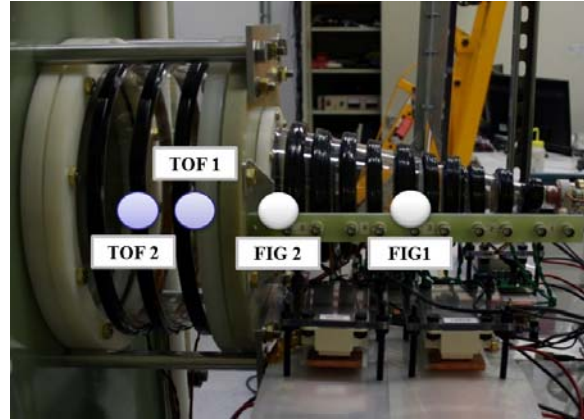


**Figure 23. Geometry of test setup. Shown are Fast Ion Gauge locations 1,2 and Downstream TOF Langmuir probe locations 1 and 2.**

Figure 25 shows a long exposure photo of an RMF-formed FRC translating into a background neutral gas region. Some increase in ionization (bright optical emission shows excitation during the ionization process) during the downstream region underneath the first acceleration coil. As can be seen in Figure 19 and Figure 24 the peak arrival of a plasma body (which is not necessarily and FRC at this location) is much later than any simple, passively ejected RMF FRC. Additionally, compared to the same diamagnetic formation signal, the peak density is approximately half. It is also worth noting that there is an initial high velocity peak and then a trailing, slower plasma mass. This effect will be discussed in further detail in the later acceleration data.

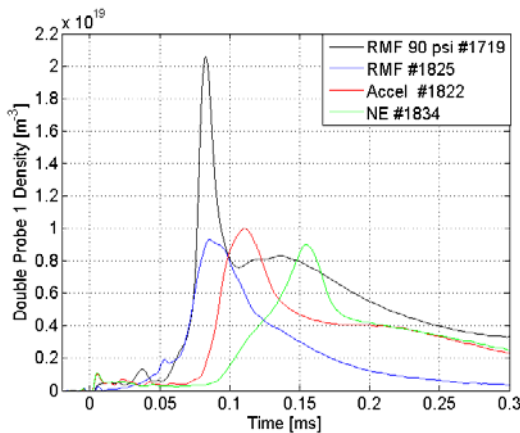


**Figure 24. Downstream double probe results for the key RMF translation conditions. Shown are two RMF formation pressures, downstream central peak arrival with a neutral gas, and downstream central peak arrive with the addition of acceleration.**

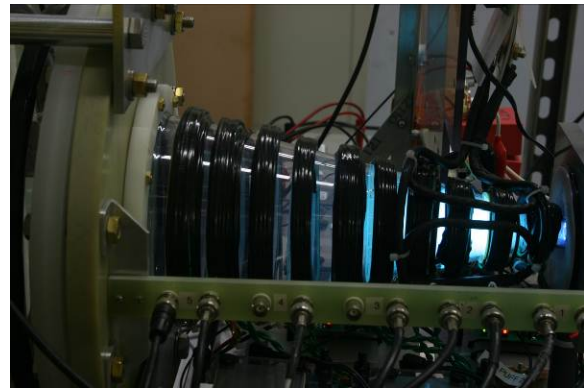


**Figure 25. Photograph of an RMF-xenon discharge with a downstream neutral gas. Minor downstream ionization is seen.**

## XENON ENTRAINMENT AND ACCELERATION

Acceleration studies were performed in order to demonstrate neutral entrainment. Ideally, the key metric for determining the success of the neutral entrainment technique was the ability to both decelerate an FRC using downstream neutral gas as well as accelerate or maintain its kinetic energy while increasing the available propellant. A variety of coil timing tests were performed. The first was a range of empirical timing studies for the first acceleration coil. This coil is situated right after the RMF formation region in order to eject the FRC at optimal temperature, density and energy without having to rely on the passive injection methods that have been performed in the past.

This study varied initial acceleration times for a moderate accelerating field. In these cases, a 2.4 kGauss field was applied as shown in the magnetic field results in Figure 26. The field has a rise time of approximately 1.5 microseconds and then was crowbarred to prevent field oscillation. Empirically, it was found that the optimal injection time to maximize final FRC velocity, as well as final diamagnetic content (the amount of excluded field from the FRC which thus implies the magnetized plasma inventory), was 18 +/- 2 microseconds after discharge initiation. This, as could be expected, optimal timing occurred at the maximum diamagnetic and plasma conditions. These results are not surprising and were as predicted and discussed earlier.

However, a more interesting study was then conducted to add the 3 further acceleration coils. A range of optimization studies were performed on the subsequent coils. For the results shown here, a linear separation is given, though MHD results show that for an accelerating FRC a more careful optimization is required. For so-called constant velocity acceleration in which mass is added at each stage as is expected in the steady flowing conditions, a linear separation is likely ideal. In this linear operation, each subsequent coil is triggered fiber-optically 2 to 20 microseconds apart and after the primary discharge. Results are shown in Figure 27 and several key scaling can be found, also expected. First, any acceleration appears to significantly accelerate the FRC, either through magnetic gradient or heat addition. If the timings are too fast, then the FRC does not eject from the device before being compressed. Essentially, instead of being pushed, it is crushed. As the FRC is a high-Beta plasma configuration, the resulting plasma is super-heated and compresses radially, increasing radial pressure. It then flows along axis and has a highly-centralized radial profile. In this case (5 microseconds), the resulting plasma has a very deformed downstream axial profile, appears highly centered on axis, is slow-moving and clearly not ideal. As the coil peak field timing then begins to follow the plasma, the FRC found downstream then accelerates and the plasma seen at the downstream double probe arriving sooner. The timing used here was found to be the maximum timing tested, trailing the FRC significantly. This implies that the FRC is rather insensitive to the discharge timing as long as it is downstream of the peak field. It is important to note that as described previously, this process is unlike a current-sheet conical acceleration as the plasma diamagnetic pressure, and thus the increase in applied magnetic field gradient, is the primary energy transfer mechanism, rather than the simple cone angle of the acceleration field coils.

Figure 28 shows a radial profile of the 20 microsecond case. Figure 29 shows a 250 ms exposure photograph of an RMF-formed FRC with acceleration through a background gas. No major increase in ionization is seen. The radial profile has several key elements of interest at this stage. First, the overall FRC appears to have expanded further radially. This was somewhat unexpected as in the MOQUI MHD modeling, the FRC was always shown to have contracted radially. Additionally, the expanded radial plasma has been greatly accelerated (compared to the non-accelerated radial profile). This expansion will have to be accounted for in later bias field design to force radial plasma contraction away from the thruster walls. Also, the central, wedge-shaped peaked profile has been reduced, or rather the large radial extents have been accelerated more than the center region. This is to be expected if there is less neutral density near the edges and unfortunately makes time of flight velocity measurements quite problematic. Perhaps most interesting is the clear transition from a single, peaked profile with just RMF to more 'spread-out' axial profile. There is a clear fast moving bulk propellant that is leaving behind a tail of slower moving plasma. This was seen somewhat in the modeling as the propellant that was lost from the closed field region. It is also possible this is an artifact of the pulsed nature of the neutral injection as

Approved for public release; distribution is unlimited.

higher density neutral gas follows the FRC out of the puff valve. Follow-on programs will seek to validate this slow moving plasma tail with a steady flowing gas. This tail will have ramifications to overall thruster performance and gas utilization, if realized in the steady flowing case. Rep-rate and overall thruster gas density will have to be optimized to maximize sweep-up.

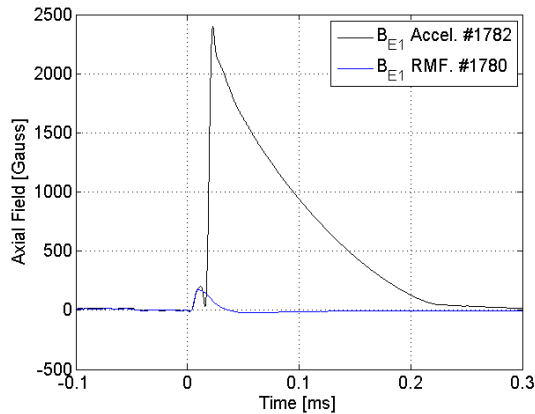


**Figure 26. Acceleration magnetic field profile for a single accelerated FRC.** Total energy of 0.75 Joules.

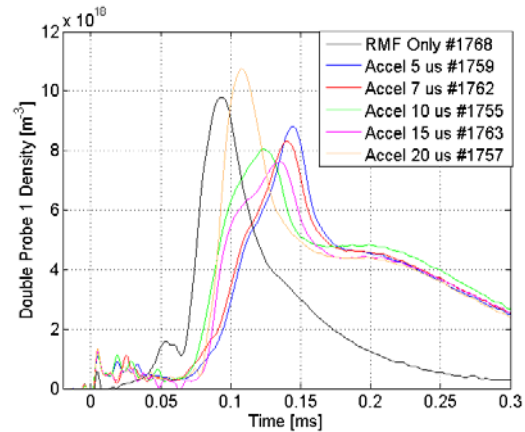


**Figure 27. Downstream double probe results for the key acceleration conditions.** Shown is obvious acceleration, over compression, and no acceleration conditions.

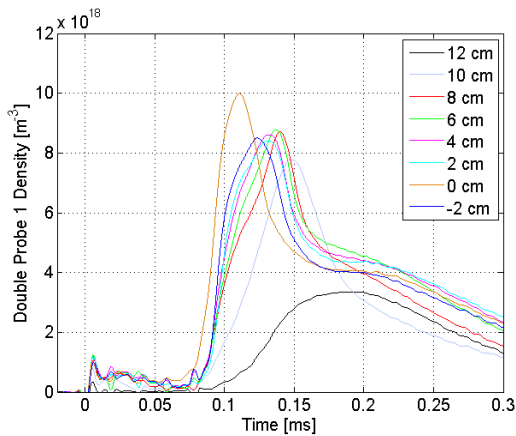


**Figure 28. Radial plasma density profile for an accelerated, entrained plasma.** Shot #1770-1842.

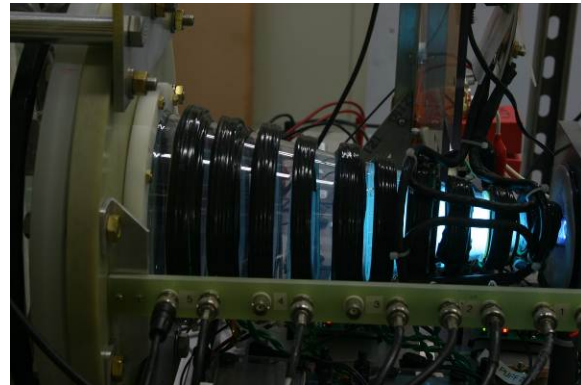


**Figure 29. Photograph of an RMF-xenon discharge with a downstream neutral gas and 2.3 Joules of acceleration.**

## CONCLUSION

A new innovation, the PROTEAN, adds a secondary Neutral Entrainment (NE) stage that, if successful, can reduce plasma formation losses in electromagnetic and electrostatic electric propulsion thrusters. This NE stage injects neutral propellant into the plasma path after ejection from an electromagnetic Field Reversed Configuration (FRC) thruster, such as the 1 kW Electromagnetic Plasmoid Thruster (EMPT). The FRC ingests these neutral particles, accelerating them up to high velocity through resonant charge exchange collisions. The NE stage then efficiently adds further kinetic energy to the engorged plasmoid through Peristaltic Dynamic Acceleration, in which sequenced theta-pinch coils are actuated to provide a large magnetic pressure gradient. Presented are results from a single-pulse experiment which show that Neutral Entrainment works as theoretically predicted for a xenon propellant. Xenon RMF-FRCs were formed, injected into a neutral gas, and then accelerated through that neutral gas. A wide range of timing and gas optimization tests were done. They showed clearly that the xenon FRCs can be decelerated significantly by the centrally-located neutral gas and then with the application of four pulsed magnetic field coils, can be accelerated back up to high velocity. This appeared to happen without wall interaction, with minor additional ionization, and no apparent increase in frozen flow losses.

## ACKNOWLEDGEMENTS

The authors would like to thank AFRL for supporting this effort, particularly Dr. Daniel Brown, Dr. Mitat Birkan, and the Phase I STTR "Propulsion Optimization of Thrust through Auxiliary Entrainment of Neutrals".

## REFERENCES

1. Jahn, R. Physics of electric propulsion, McGraw-Hill, 1968.
2. Lieberman, M. and A. Lichtenberg. Principles of plasma discharges and materials processing, Wiley, 2005.
3. Tuszewski, M. "Field reversed configuration plasmas". Nuclear Fusion, 28:2033, 1988.
4. Slough, J.T. and Miller, K.E., "Flux generation and sustainment of a field reversed configuration with rotating magnetic field current drive", Phys. Plasmas 7, 1945 (2000).
5. Matsuzawa, Y., et. al, "Effects of background neutral particles on a field-reversed configuration plasma in the translation process". Physic of Plasmas 15 (2008).
6. Rabb, D. and W. Francis. "Charge exchange between gaseous ions and atoms." The Journal of Chemical Physics 37: 2631, 1962.
7. Smirnov, Boris M. Physics of atoms and ions. Springer, 2003.
8. Brackbill, Jeremiah, et al. "Ionization and Charge Exchange Reactions in Neutral Entrainment of a Field Reversed Configuration Thruster." (2012).
9. Meier, E.T., et al. "Development and validation of a two-fluid plasma-neutral model", Innovative Confinement Concepts (2011).
10. Glasser, A.H. and Tang, X.Z., "The SEL macroscopic modeling code", Comput. Phys. Commun. 164, 237 (2004).
11. Slough, J., Blair, A., Pihl, C., and Votroubek, G., "Magnetically Accelerated Plasmoid (MAP) Thruster", IEPC-2007-16, The 30th IEPC, Florence, Italy, Sept. 17-20, 2007.
12. Kirtley, D. et al. "Pulsed Plasmoid Propulsion: Air-Breathing Electromagnetic Propulsion". IEPC-2011-15, International Electric Propulsion Conference, Wiesbaden 2011.

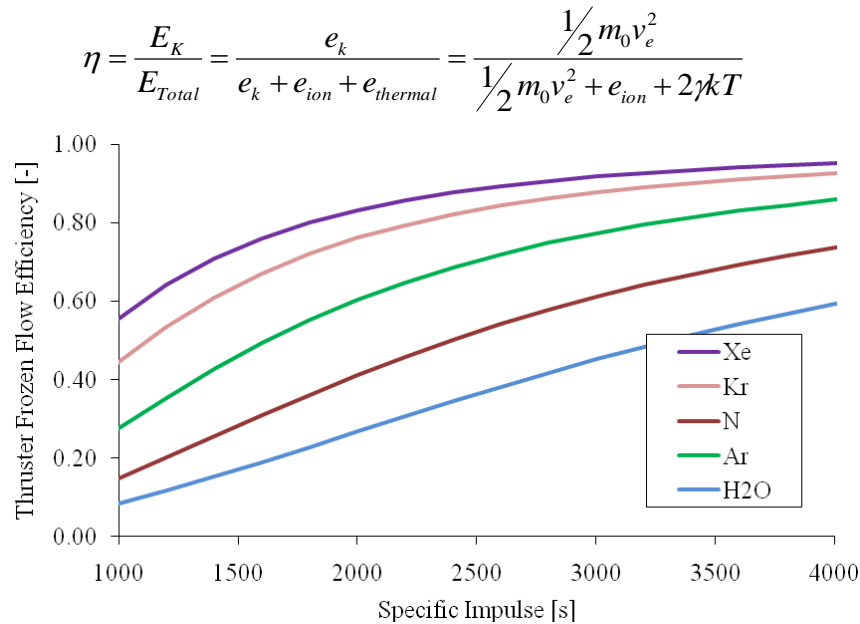
# NEUTRAL ENTRAINMENT DEMONSTRATION IN A XENON FRC THRUSTER EXPERIMENT

David Kirtley, George Votroubek, Anthony Pancotti, Jim Pihl  
*MSNW LLC, Redmond, WA.*

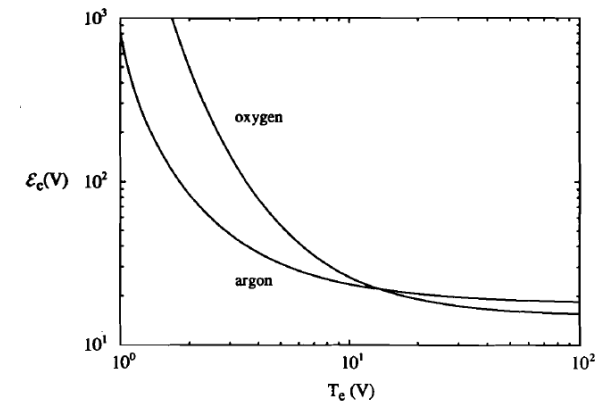
John Slough  
*The University of Washington, Seattle, WA*

Real plasma-based propulsion systems take 5-10X minimum ionization energy to actually form and eject a plasma

Electrostatic and Electromagnetic systems pay a large efficiency penalty to operate on lightweight gases (also T/P for heavy gases)



Theoretical maximum thruster efficiency with a 40 eV/ion frozen flow (plasma formation) loss



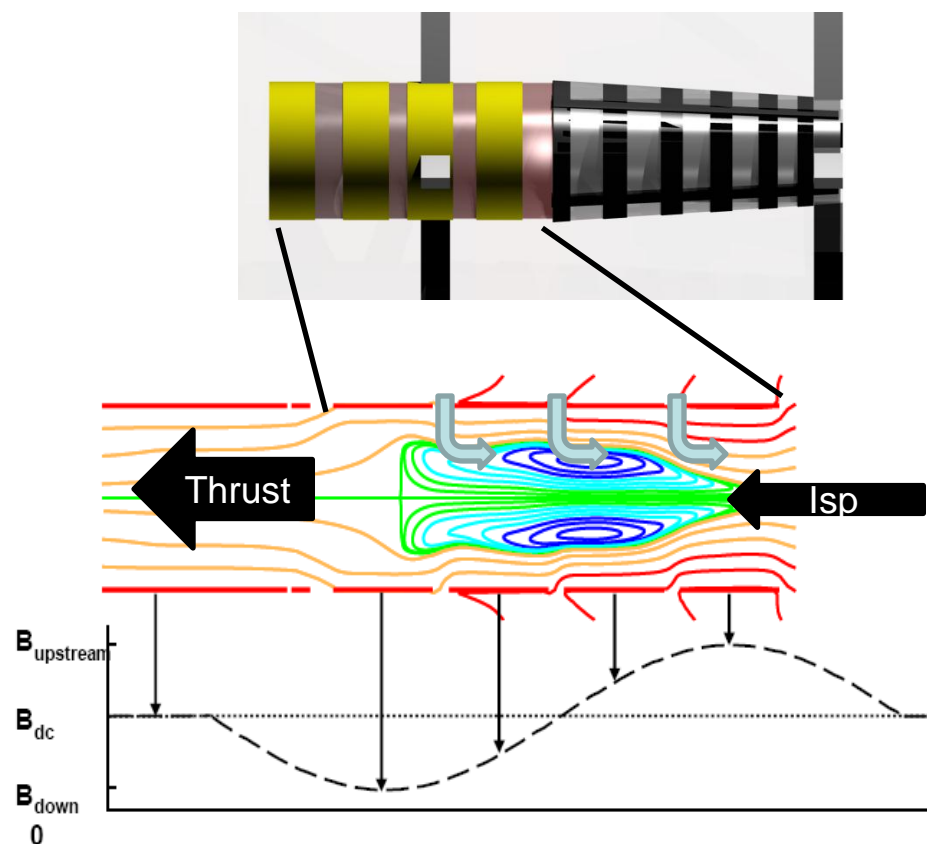
**How can we accelerate lightweight, chemically reactive gases, but without the large ionization costs?**

**ISSUE:** Plasma formation is the primary loss mechanism for ALL electrostatic or electromagnetic propulsion systems. It prevents operation at lower specific impulse, lowers efficiency at all exit velocities, and requires high mass propellants.

**Solution:** Entrain neutrals in an acceleration field *after* formation.

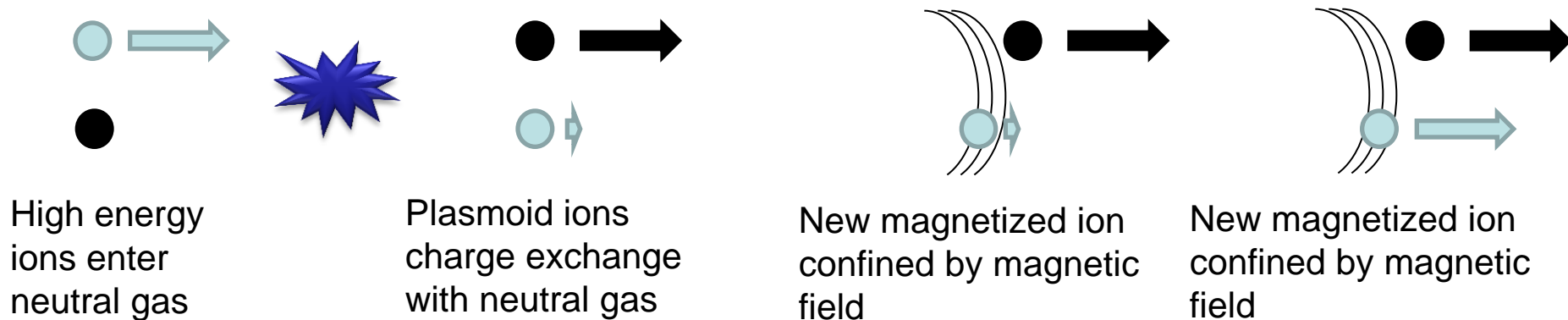
**Benefit:** Specific impulse can be tailored to the mission, while the thruster operated at its maximum efficiency, even on light propellants.

- **Basic Idea:** An FRC will 'inject' large quantities of neutral gas through charge exchange collisions, not ionization. If you accelerate an FRC while providing upstream neutral gas,  $I_{sp}$  can be specified and mass/thrust added with very high efficiency [1].



[1] Matsuzawa, Y., et. al, "Effects of background neutral particles on a field-reversed configuration plasma in the translation process". Phys. Plasmas 15, (2008).

## Entrainment of Neutrals in a Magnetized Plasma

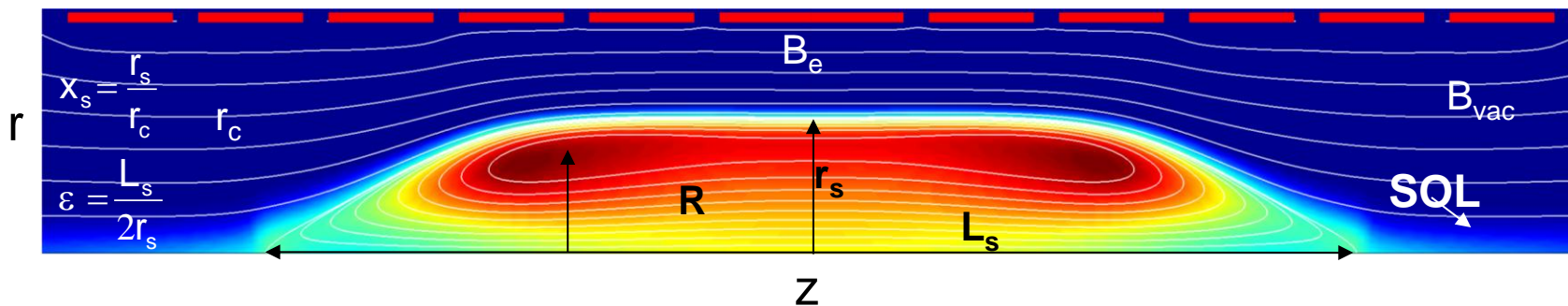


- Charge exchange collisions dominate
- Ionization must be minimal
- Gas utilization is key

*Effectively accelerate neutrals rather than ions*

# Field Reversed Configuration (FRC)

## Magnetic Field lines and Pressure Contours



**Key  
Equilibrium  
Relations:**

$$\left\{ \begin{array}{l} B_{\text{ext}} = \frac{B_{\text{vac}}}{1 - x_s^2} \\ P_0 = n_0 kT = \frac{B_{\text{ext}}^2}{2\mu_0} \\ \langle \beta \rangle = 1 - \frac{1}{2} x_s^2 \end{array} \right.$$

### Flux Conservation

External measurements of B yield  
FRC separatrix radius  $r_s(z)$ , FRC length  $L_s$   
 $\Rightarrow$  volume, position, velocity

### Radial Pressure Balance

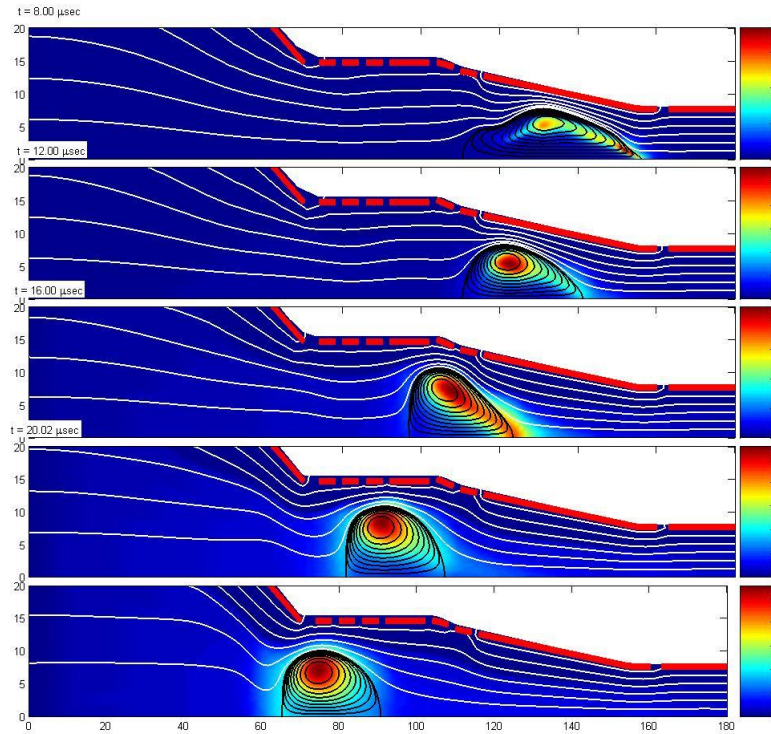
Simple cross-tube interferometric  
measurement with  $r_s$  from yields  $\langle n \rangle$  and T

### Axial Pressure Balance

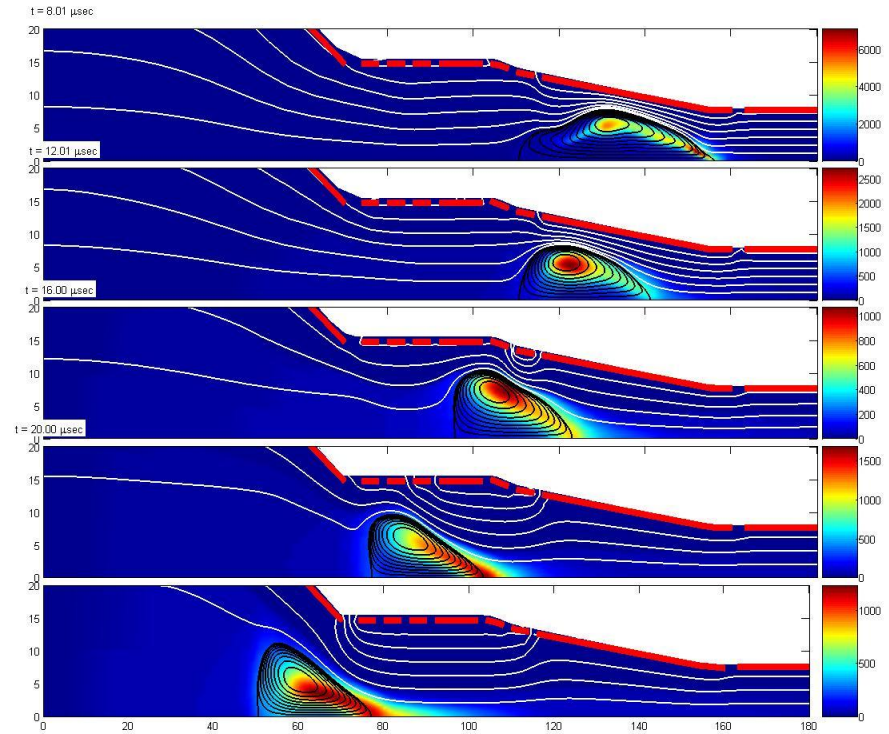
With above obtain plasma energy,  
Inventory, confinement times

FRC equilibrium constraints and the diagnostic measurements that together with the equilibrium relations that are employed to determine the basic parameters of the FRC equilibrium

Standard FRC Thruster Operation



FRC thruster with sequenced coil array



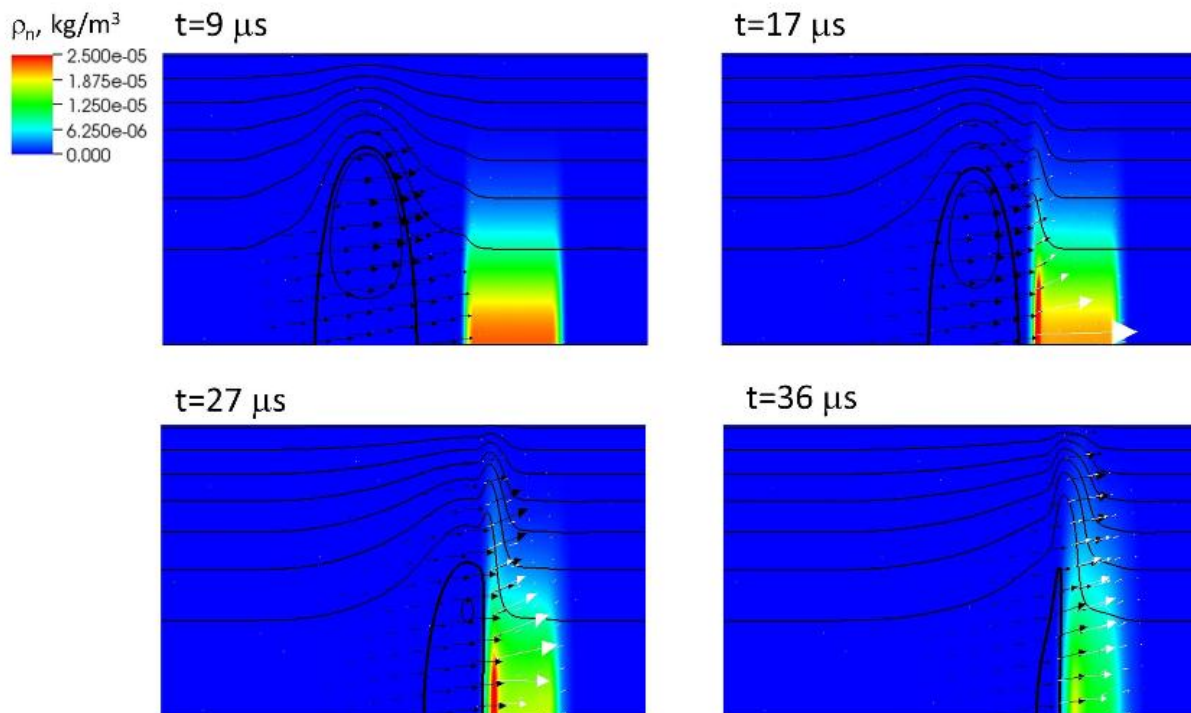
“Afterburner” following current FRC thruster accelerates FRC through peristaltic electromagnetic acceleration

Increase total  $dM/dx$  through multiple field coils

# Ion - Neutral Interaction

## Employing the SEL Code

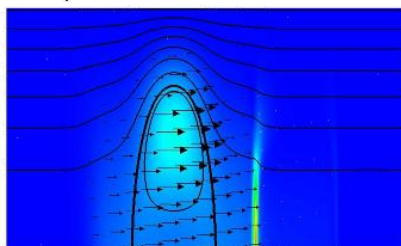
- SEL-HiFi Visco-Resistive MHD
  - Neutral and Ion Fluids added
  - Flux-source form for inputs
  - Completely implicit with an adaptive grid with high-order spectral elements
- Neutral fluid with resonant charge exchange, electron-impact ionization, and radiative recombination reactions



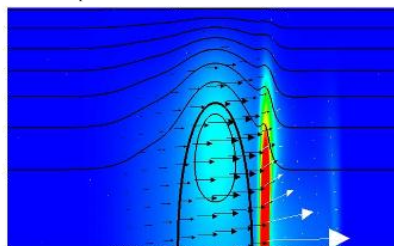
**Neutral density pseudocolor plots for baseline ELF simulation with a Gaussian radial neutral gas profile.** Black and white arrows indicate the direction and magnitude of plasma and neutral momentum, respectively. Clear neutral entrainment is seen.

Meier, E.T., et al. "Development and validation of a two-fluid plasma-neutral model", Innovative Confinement Concepts (2011).

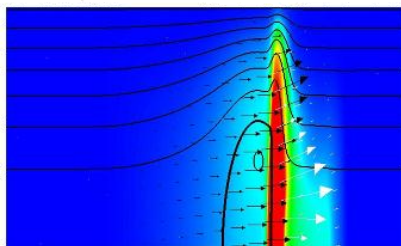
$t=9 \mu\text{s}$



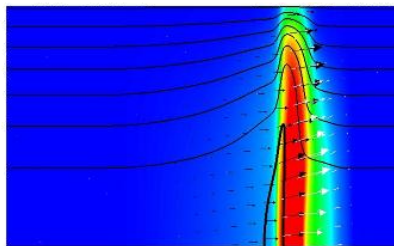
$t=17 \mu\text{s}$



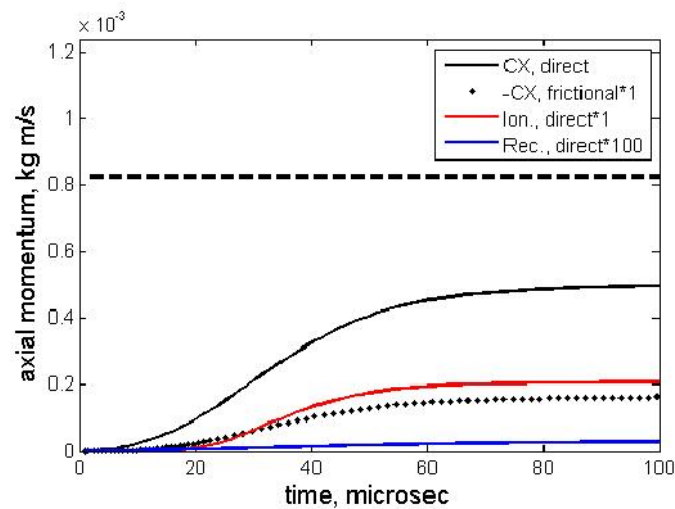
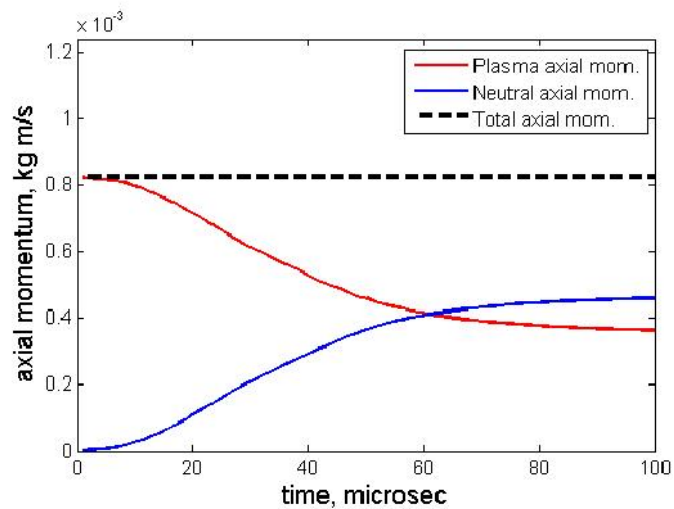
$t=27 \mu\text{s}$



$t=36 \mu\text{s}$

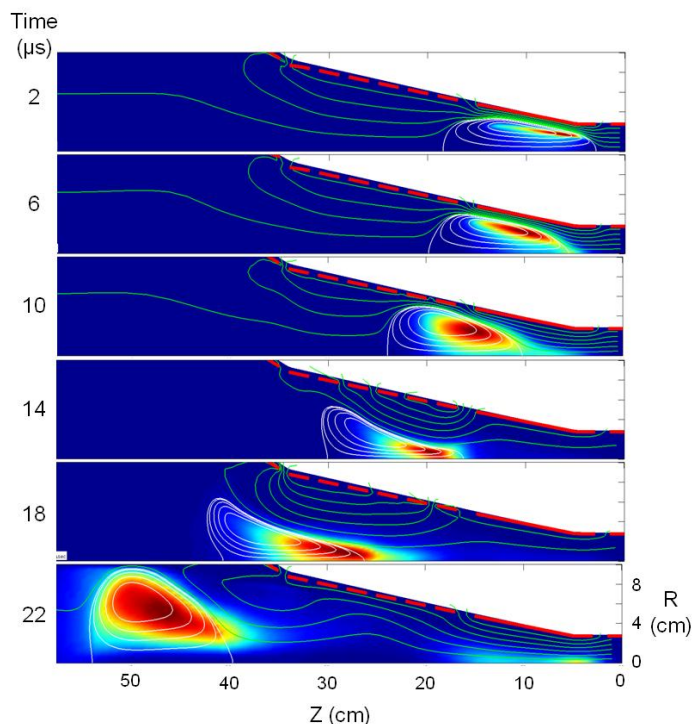


**Pressure pseudocolor plots for baseline ELF simulation.** Clear neutral entrainment, pulse sharpening, and increase in external magnetic field pressure are seen.

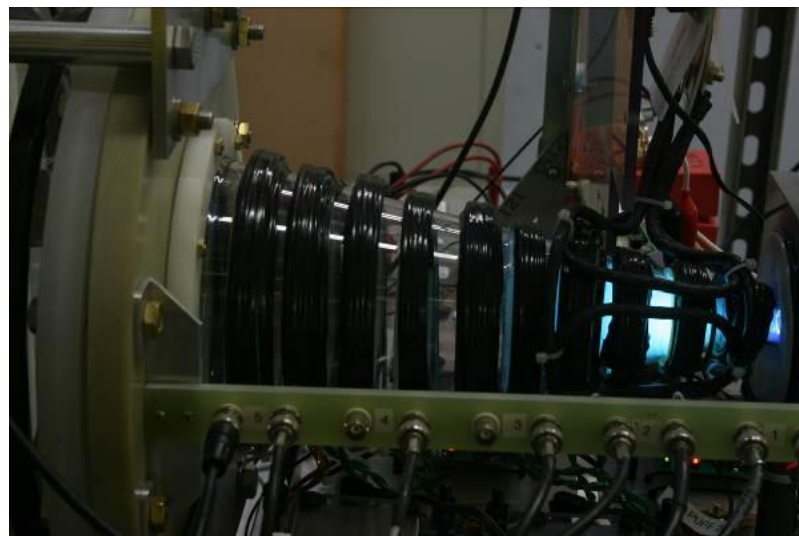


**Temporal profiles of momentum-related quantities for ELF baseline simulation**

1. Neutral Entrainment demonstrated as part of the AFOSR MACEEP program
2. Phase I of PROTEAN to demonstrate neutral entrainment in a thruster-like environment
3. Demonstrate entrainment, deceleration, and magnetic acceleration



MOQUI modeling of a Conical acceleration section with an RMF FRC

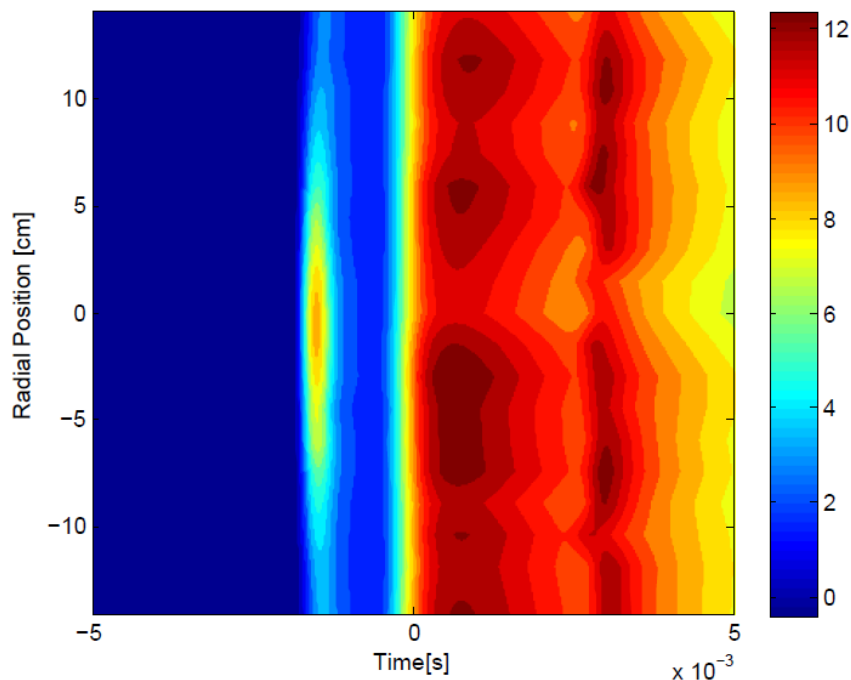


PROTEAN Phase I. Shown is a Xenon FRC.

## SCIENTIFIC CHALLENGES:

- Predict and experimentally validate the velocity and density limitations of neutral entrainment in a thruster application
- Quantify effects of charge exchange and ionization with an easily ionized and thruster relevant gas (Xenon)

- Neutrals injected on axis and in limited axial location to isolate effects
- Supersonic Molecular Beam Injector designed and implemented
- Clear beam formed with  $\pm 3$  degree ejection angle
- Coaxial neutral beam injector and tangential swirl pre-ionization injector

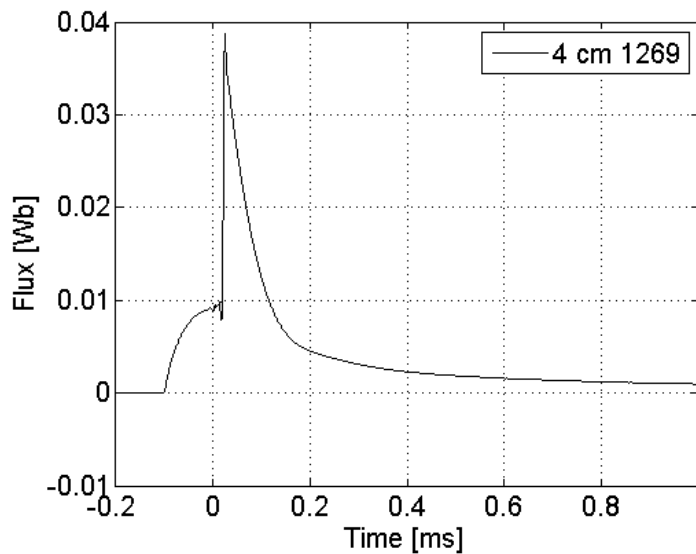


**Neutral Density profile in mT for the discharge of interest showing initial neutral beam and follow-on FRC propellant flows at 68 cm.**



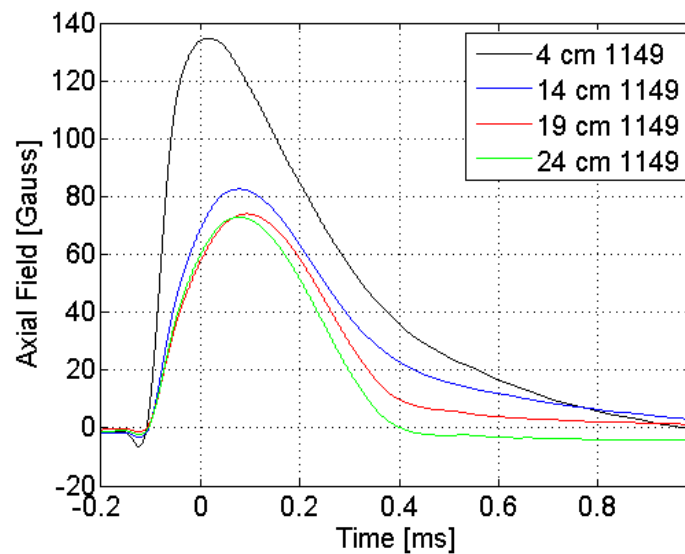
**Coaxial SMBI and pre-ionization electrode**

- Combined bias and accelerator circuits
- Capable of simple energy recovery
- 5 total bias field an accelerator coils
- 50 – 200 G, 10 ms bias with 500 – 3000 G, 3  $\mu$ s accelerators



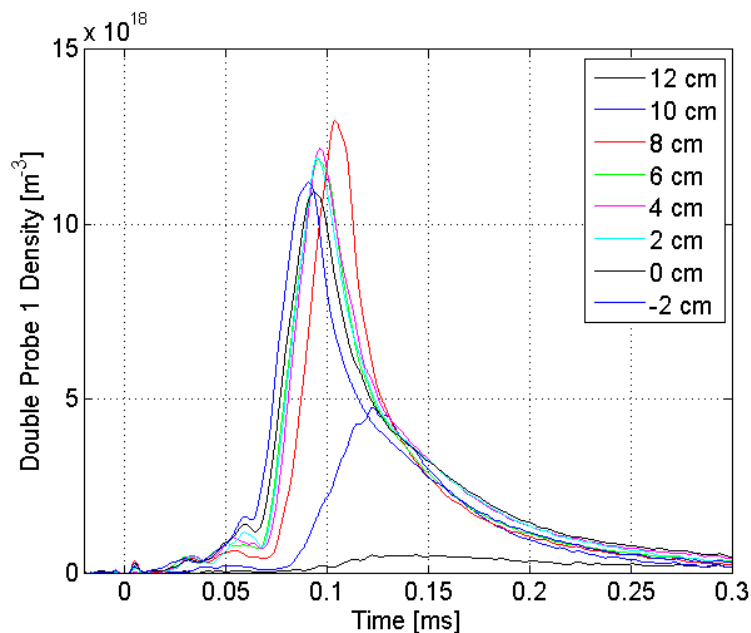
**Magnetic flux measurement with the primary accelerator coil.**

Shown is 5 V bias and 100 V acceleration capacitor banks.

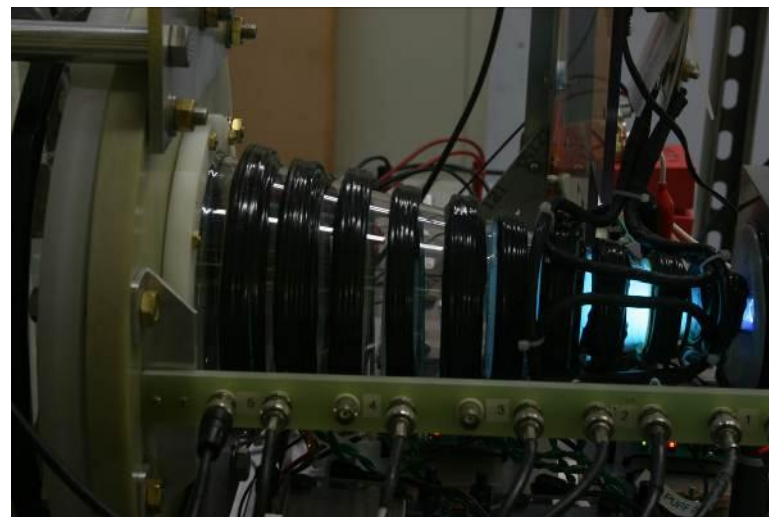


**Composite magnetic field profiles for all four bias field discharges.** Axial probe location is indicated. Shot #1149.

- 2.8 J, 300 kHz RMF formation
- FRC formed and passively translated downstream
- Expected downstream velocities and arrival times measured with TOF double Langmuir probes
- Gas only injected with outer formation injector (swirl)

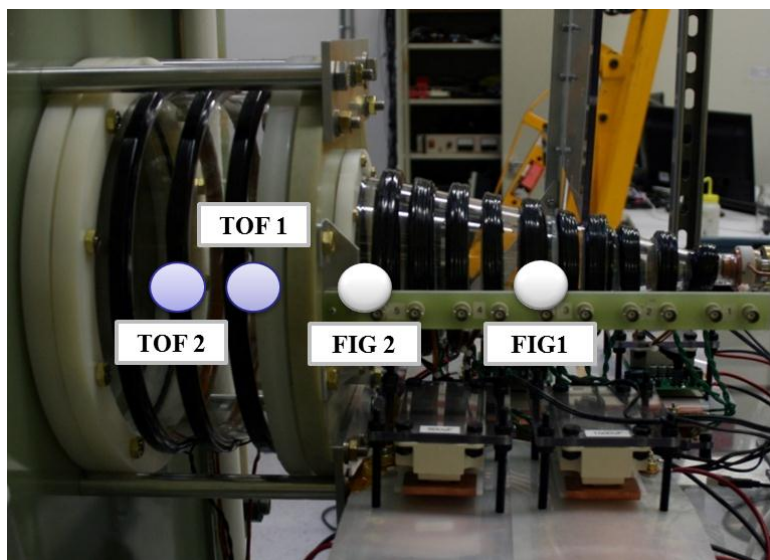


**RMF Radial profile.** Shot #1770-1842.

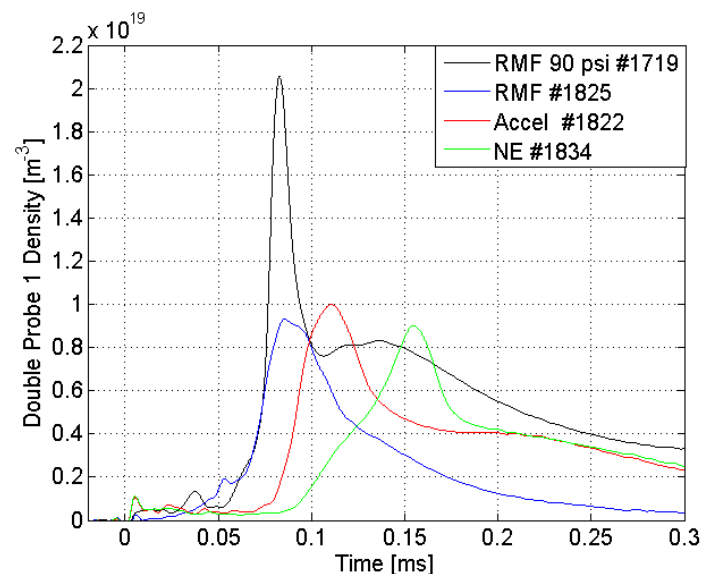


**Photograph of an RMF-xenon discharge at approximately 2.8 Joules.** Annular pre-ionization and localized ionization region is clear.

- Internal neutral beam added
- Downstream profiles matched (as much as possible) between only formation gas injection (outer swirl) and inner neutral beam injection
- Clear deceleration and apparent entrainment
- No increase in downstream density or optical radiation (ionization)
- Radial and axial expansion and ‘smearing’ of FRC profile

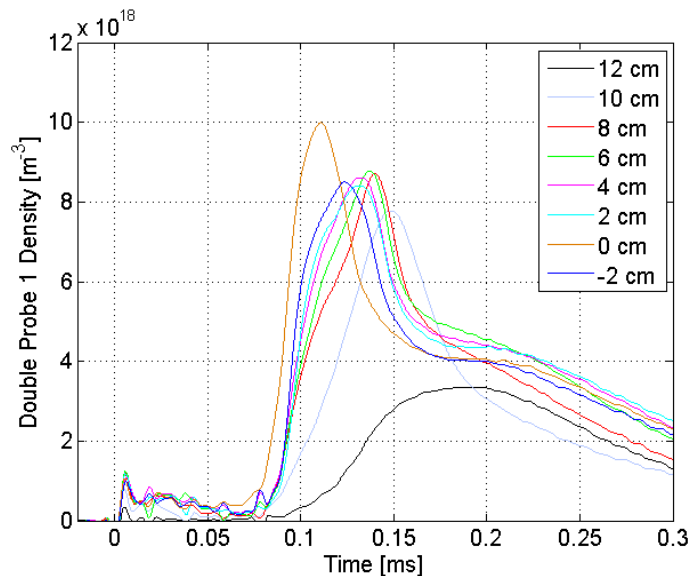


Geometry of test setup. Shown are Fast Ion Gauge locations 1,2 and Downstream TOF Langmuir probe locations 1 and 2

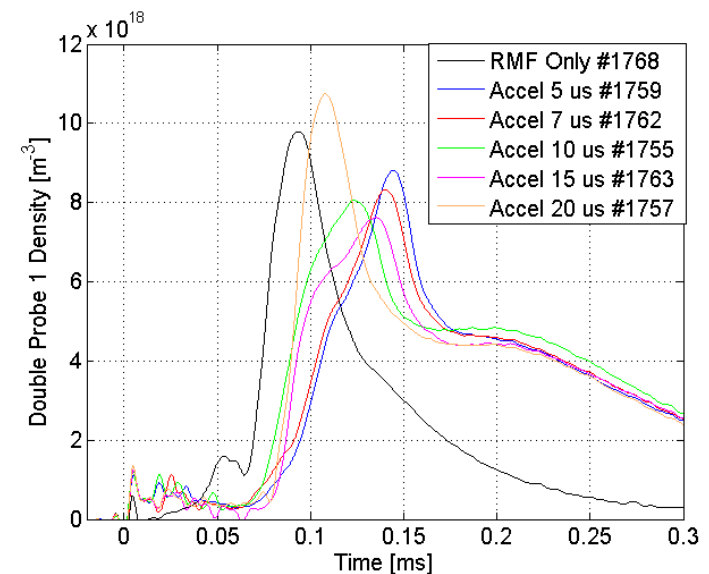


Downstream double probe results for the key RMF translation conditions. Shown are two RMF formation pressures, downstream central peak arrival with a neutral gas, and downstream central peak arrive with the addition of acceleration.

- Acceleration fields added to decelerated profile - 2.4 kG, 2.3 Joules
- Single initial acceleration in formation region optimized 18 microseconds after discharge initiation (slightly past peak diamagnetic signal).
- 3 secondary acceleration coils added with uniform spacing (5-20 microseconds)
- FRC could be accelerated back up to initial, non-entrained velocity
- Optimal timing was surprisingly late, i.e. peak field always trails peak diamagnetic signal (both geometrically and temporally)
- Apparent increase in slow moving tail plasma, transient gas injection is likely culprit

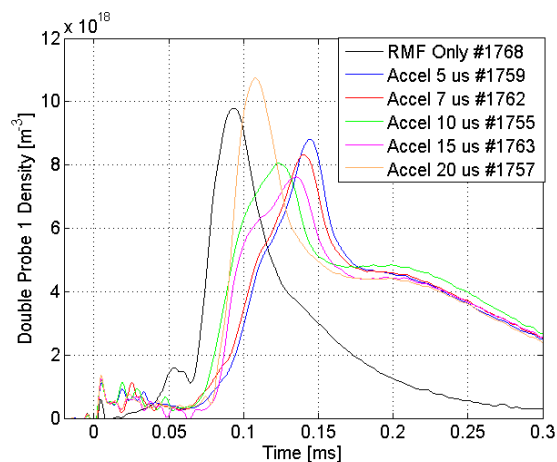


**Radial plasma density profile for an accelerated, entrained plasma. Shot #1770-1842.**

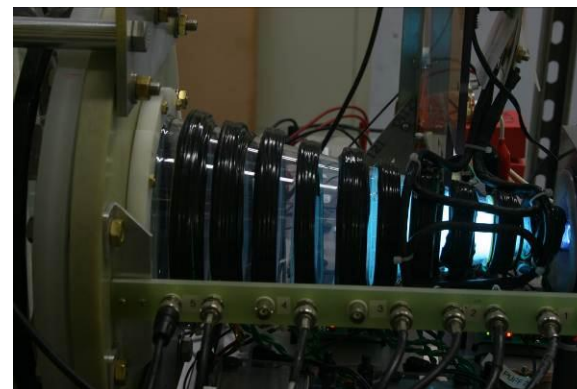


**Downstream double probe results for the key acceleration conditions. Shown is obvious acceleration, over compression, and no acceleration conditions.**

- Neutral Entrainment has the capability to reduce effective plasma frozen flow losses in electromagnetic propulsion systems
- The PROTEAN test bed was built and demonstrated Xenon and Argon FRCs
- Combined pulsed magnetic bias fields with peristaltic acceleration demonstrated
- Xenon operated with low-pressure (temperature) FRCs showed little ionization
- Transient gas injection lead to radial and axial expansion and gas under-utilization
- Xenon RMF-FRCs were formed, injected into a neutral gas, and then accelerated.
- Xenon FRCs can be decelerated by the centrally-located neutral gas and with the four pulsed magnetic field coils, can be accelerated back up to high velocity.



**Downstream double probe results for the key acceleration conditions.** Shown is obvious acceleration, over compression, and no acceleration conditions.

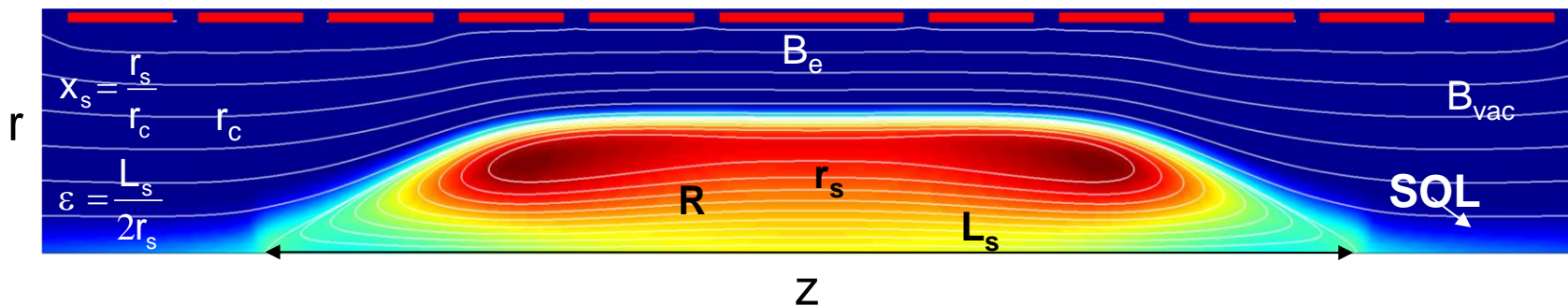


**Photograph of an RMF-xenon discharge with a downstream neutral gas and 2.3 Joules of acceleration.**

# BACKUP – Neutral Entrainment

# Field Reversed Configuration (FRC)

## Magnetic Field lines and Pressure Contours



**Key  
Equilibrium  
Relations:**

$$B_{\text{ext}} = \frac{B_{\text{vac}}}{1 - x_s^2}$$

$$P_0 = n_0 kT = \frac{B_{\text{ext}}^2}{2\mu_0}$$

$$\langle \beta \rangle = 1 - \frac{1}{2} x_s^2$$

### Flux Conservation

External measurements of B yield  
FRC separatrix radius  $r_s(z)$ , FRC length  $L_s$   
 $\Rightarrow$  volume, position, velocity

### Radial Pressure Balance

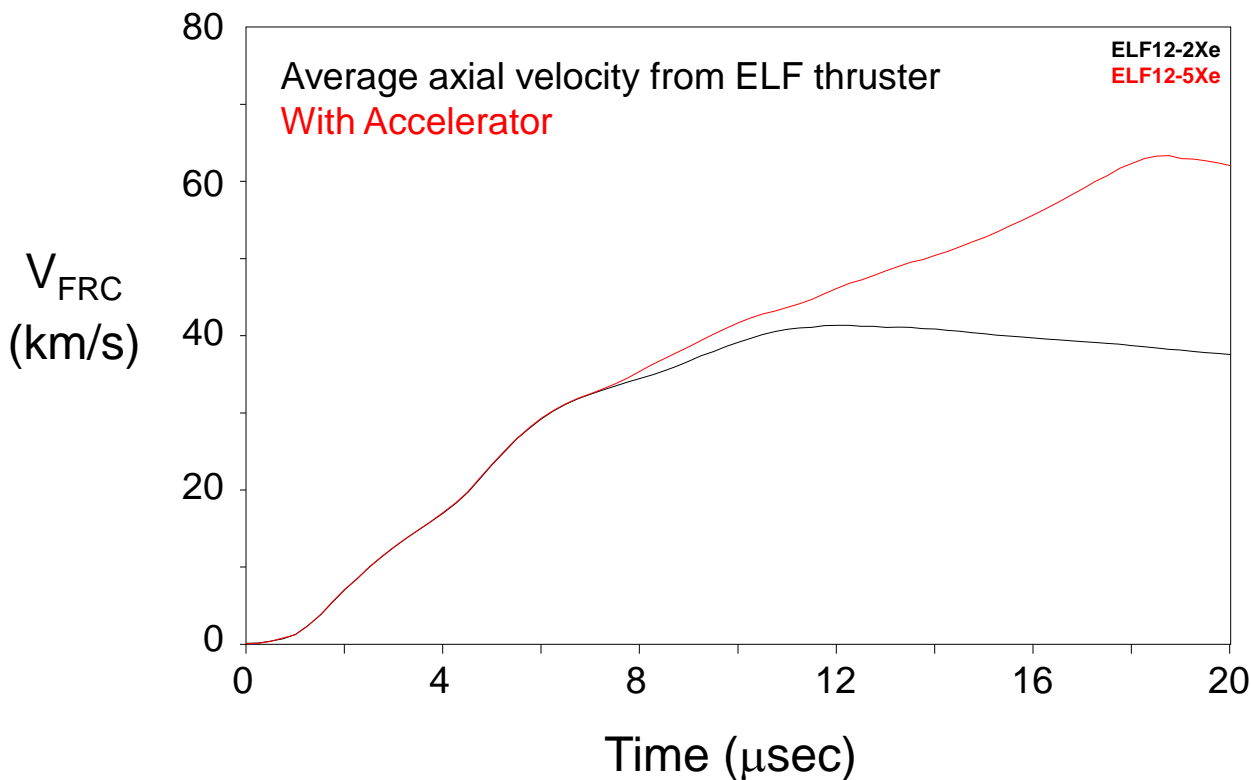
Simple cross-tube interferometric  
measurement with  $r_s$  from yields  $\langle n \rangle$  and T

### Axial Pressure Balance

With above obtain plasma energy,  
Inventory, confinement times

FRC equilibrium constraints and the diagnostic measurements that together with the equilibrium relations that are employed to determine the basic parameters of the FRC equilibrium

# Increase in FRC Isp with Follow-on Magnetic Accelerator

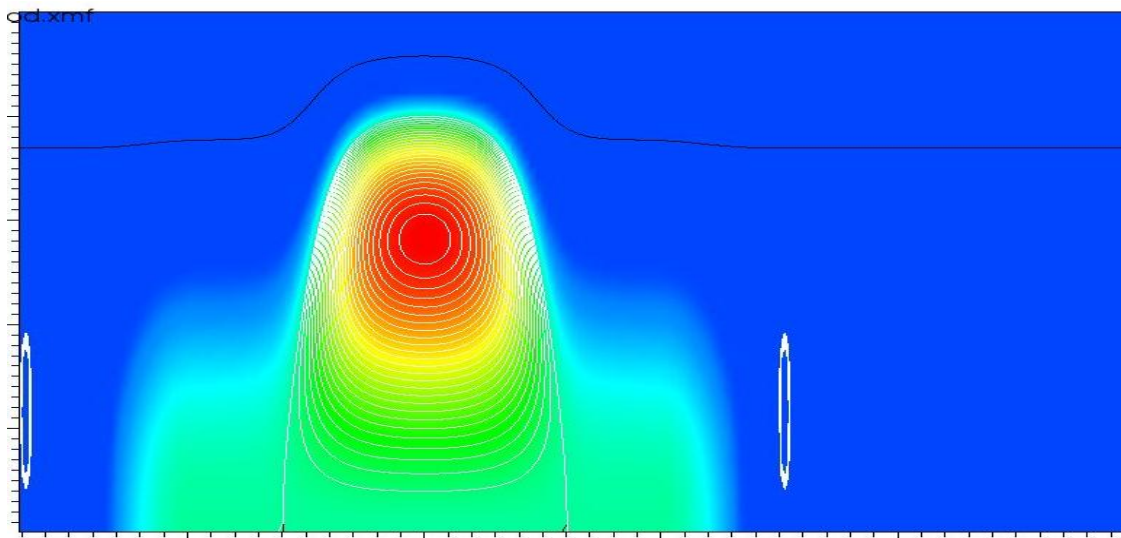
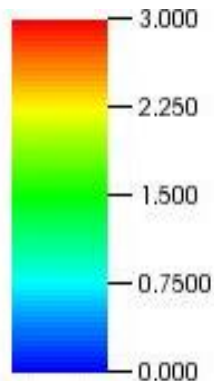


Kinetic energy gain observed with accelerator would be employed to maintain FRC Isp during entrainment i.e.

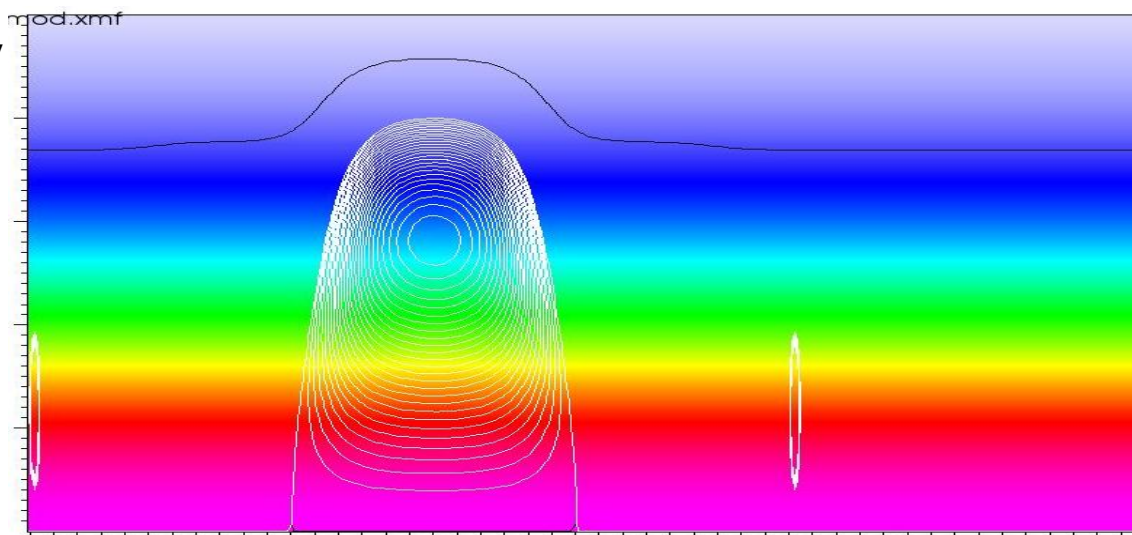
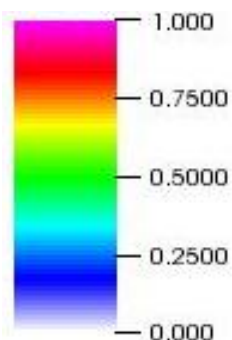
$$F = \dot{m} V_{FRC} \quad \text{rather than} \quad F = m \dot{V}_{FRC}$$

# 2D Numerical Calculation of Ion - Neutral Interaction Employing the SEL Code – Initial conditions

D Ion Density  
( $\times 10^{19} \text{ m}^{-3}$ )

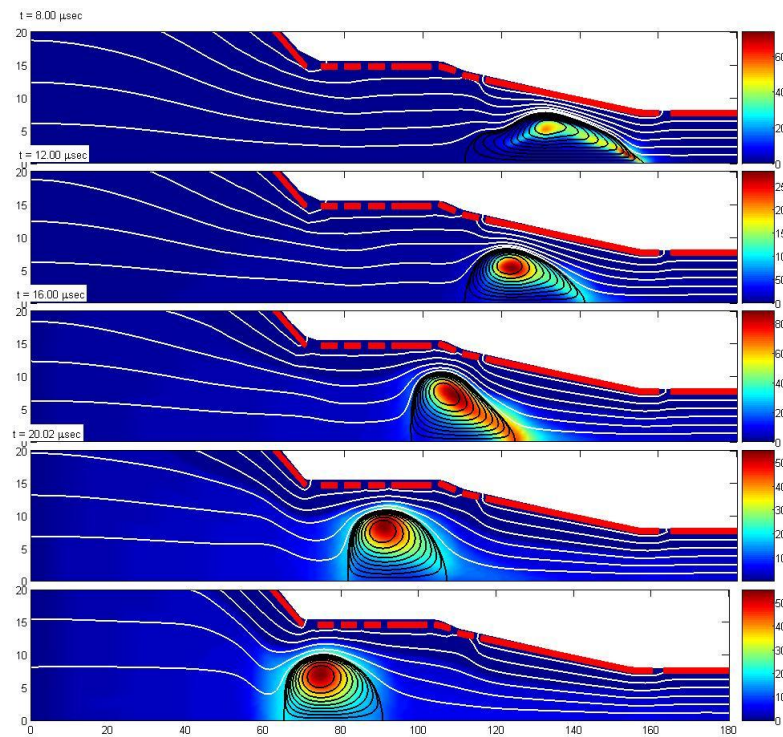


D Neutral Density  
( $\times 10^{19} \text{ m}^{-3}$ )

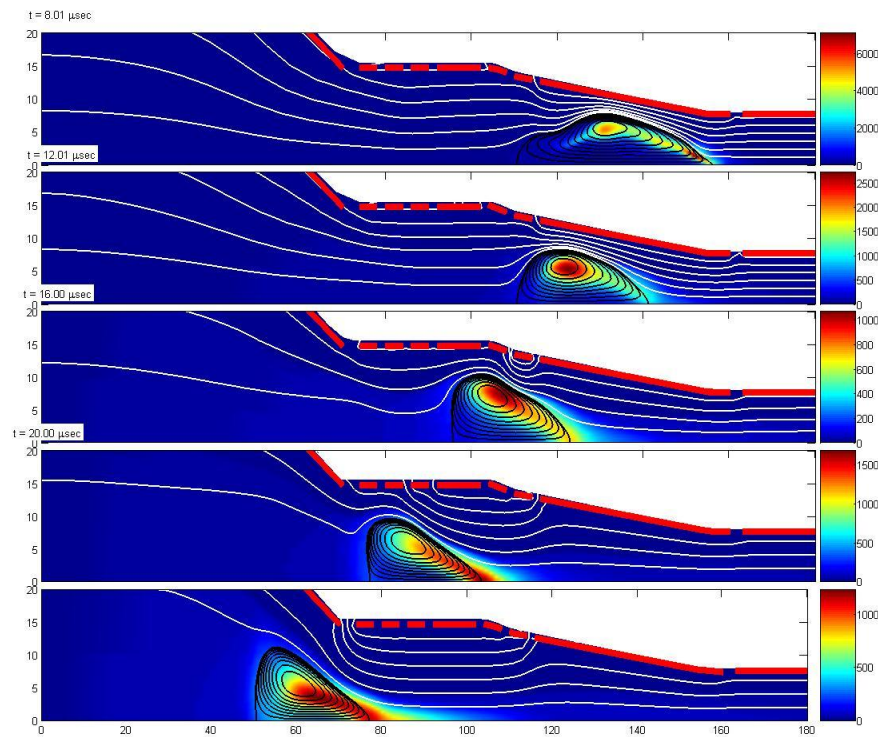


# 2D Resistive Calculation for Entrainment Experiments with ELF thruster

Standard ELF Thruster Operation



ELF thruster with sequenced coil array



“Afterburner” following current ELF thruster would be used to increase thrust at constant  $I_{sp}$  at very high efficiency with neutral entrainment

# SEL Implementation of Visco-Resistive MHD with a Dynamic Neutral Fluid Background

## Density Equations

$$\frac{\partial \rho_i}{\partial t} + \nabla \cdot (\rho_i \mathbf{v}_i) = m_i (\Gamma_{ion} - \Gamma_{rec})$$

$$\frac{\partial \rho_n}{\partial t} + \nabla \cdot (\rho_n \mathbf{v}_n) = m_i (\Gamma_{rec} - \Gamma_{ion})$$

## Momentum Equations

$$\frac{\partial}{\partial t} (\rho_i \mathbf{v}_i) + \nabla \cdot (\rho_i \mathbf{v}_i \mathbf{v}_i + p \tilde{\mathbf{I}}) = \mathbf{j} \times \mathbf{B} - \Gamma_{rec} m_i \mathbf{v}_i + \Gamma_{ion} m_i \mathbf{v}_n + \Gamma_{cx} (m_i \mathbf{v}_n - m_i \mathbf{v}_i)$$

$$\frac{\partial}{\partial t} (\rho_n \mathbf{v}_n) + \nabla \cdot (\rho_n \mathbf{v}_n \mathbf{v}_n + p_n \tilde{\mathbf{I}}) = \Gamma_{rec} m_i \mathbf{v}_i - \Gamma_{ion} m_i \mathbf{v}_n + \Gamma_{cx} (m_i \mathbf{v}_i - m_i \mathbf{v}_n)$$

$$\frac{1}{\gamma-1} \frac{\partial p}{\partial t} + \nabla \cdot \left( \frac{\gamma}{\gamma-1} p \mathbf{v}_i \right) = \mathbf{v}_i \cdot \nabla p + (\Gamma_{cx} + \Gamma_{ion}) (KE_n + KE_i - m_i \mathbf{v}_i \cdot \mathbf{v}_n) + \Gamma_{ion} (KE_n - \phi_{ion})$$

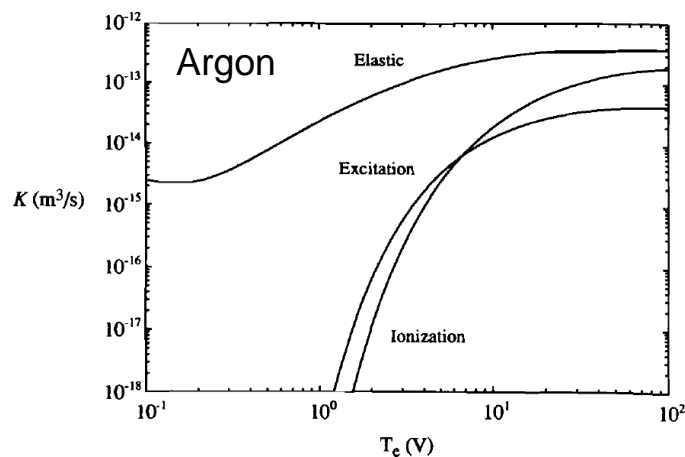
## Energy Equations

$$\begin{aligned} \frac{1}{\gamma-1} \frac{\partial p_n}{\partial t} + \nabla \cdot \left( \frac{\gamma}{\gamma-1} p_n \mathbf{v}_n \right) &= \mathbf{v}_n \cdot \nabla p_n \\ &+ \Gamma_{rec} (KE_i + KE_n - m_i \mathbf{v}_n \cdot \mathbf{v}_i - \phi_i) + \Gamma_{cx} (KE_i + KE_n - m_i \mathbf{v}_n \cdot \mathbf{v}_i) \end{aligned}$$

- Single-fluid plasma model which allows for Spitzer-Chodura resistivity, Braginskii thermal conduction, symmetric viscosity, and dissipation
- For readability, dissipative terms are excluded.

# Atomic Physics Rates

The equations being used for atomic physics rates are



$$\Gamma_{cx} = 2 * 54.82 * 10^{-20} T_{eV}^{-.2057} * v_{in} n_n n_i \frac{1}{m^3 s},$$

$$\Gamma_{ion} = \frac{2 * 10^{-13}}{6 + T_{eV} / \phi_{ion}} \left( \frac{T_{eV}}{\phi_{ion}} \right)^{1/2} e^{-\phi_{ion} / T_{eV}} n_i n_n \frac{1}{m^3 s},$$

$$\Gamma_{rec} = 7 * 10^{-20} n_i^2 \left( \frac{\phi_{ion}}{T_{eV}} \right)^{1/2} \frac{1}{m^3 s},$$

where the ion-neutral relative velocity,  $v_{in}$ , is computed from

$$v_{in} = \left( \frac{2}{m_i} k T_i \right)^{1/2} \frac{m}{s}.$$

- It is assumed that the radiation after recombination,  $h\nu$ , is immediately released and is equal to  $\phi_{ion}$ . It is also assumed that  $m_i = m_n$
- The equation for charge exchange is based on a curve fit of data in the 1966 NASA Technical Note by Nichols and Witteborn

- The KEY idea: A price in efficiency MUST be paid to operate in a lower mass gas. Fundamental physics.
- There are desirable mission reasons to be able to use air gases, i.e. no more rocket equation

## ***Assumptions in Model and Previous Graphs***

- Frozen flow losses are conservative:
  - 40 eV/ion plasma formation, radiation, ionization, wall losses, etc. (worse than measured)
  - 10 eV total residual plasma temperature ( $T_e + T_i$ ). (worse than measured)
- System-level losses:
  - 95% PPU efficiency (better than measured, but demonstrated elsewhere)
  - 95% Pulsed inductive energy addition with IGBT switching (not demonstrated, but modeled)
- Neutral entrainment CE efficiency :
  - 100 % Resonant Charge Exchange (small changes would be expected for non-resonant charge exchange with O2 to be explored via model)
  - N is number of charge exchanges per initial FRC ion
- Current Thruster Data
  - Uncertainties are both shot-to-shot and absolute measurement uncertainty
  - Thruster efficiency does not include PPU losses and uses measured downstream velocity and impulse

$$\eta_T = \eta_{PPU} \frac{E_K}{E_{FF} + E_K} = \eta_{PPU} \frac{E_{k-ELF} + NE_{k-NE}}{E_{FF} + E_{k-ELF} + NE_{k-ELF}}$$

$$\eta_T = \eta_{PPU} \frac{e_{k-ELF} + \eta_{CE}\eta_{NE}Ne_k}{e_{ion} + e_{thermal} + e_{k-ELF} + \eta_{CE}\eta_{NE}Ne_k}$$